Ore Geology Reviews 72 (2015) 373–390

Contents lists available at ScienceDirect

Ore Geology Reviews

journal homepage: www.elsevier.com/locate/oregeorev

Geological setting and timing of the world-class Sn, Nb–Ta and Li mineralization of Manono-Kitotolo (Katanga, Democratic Republic of Congo)

S. Dewaele [a,*], N. Hulsbosch [b], Y. Cryns [b], A. Boyce [c], R. Burgess [d], Ph. Muchez [b]

[a] Department of Geology and Mineralogy, Royal Museum for Central Africa, Leuvensesteenweg 13, B-3080 Tervuren, Belgium
[b] Geodynamics and Geofluids Research Group, Department of Earth and Environmental Sciences, KU Leuven, Celestijnenlaan 200E, B-3001 Leuven, Belgium
[c] Scottish Universities Environmental Research Centre, Rankine Avenue, East Kilbride G75 0QF, Scotland, UK
[d] University of Manchester, School of Earth, Atmospheric and Environmental Sciences, Oxford Road, Manchester M13 9PL, UK

ARTICLE INFO

Article history:
Received 27 March 2015
Received in revised form 8 July 2015
Accepted 11 July 2015
Available online 30 July 2015

Keywords:
Columbite–tantalite
Cassiterite
Kibara belt
Manono-Kitotolo
Pegmatite
Spodumene

ABSTRACT

The Central African Mesoproterozoic Kibara belt in Katanga (DRCongo) forms a metallogenic province that hosts a variety of granite-related mineralization, rich in cassiterite, columbite–tantalite, wolframite/ferberite, spodumene and beryl. This mineralization is mainly present in pegmatites and quartz veins that are thought to be associated with the youngest granite generation in the Kibara belt (i.e., so-called "E-group" granite generation). Manono-Kitotolo is one of the world's largest Sn, Nb–Ta and Li mineralized pegmatites, with a large resource of spodumene, columbite–tantalite and cassiterite still remaining. Mineralized pegmatites have intruded along the foliation in the Mesoproterozoic metasedimentary rocks and dolerites of the Manono-Kitotolo area. The pegmatites have been emplaced very late during the climax of the Kibaran orogeny, probably during the transition from orogenic collapse to extensional tectonics, based on their structural position. The emplacement of the pegmatites resulted in an intense alteration of the doleritic and metasedimentary host-rocks, resulting in muscovitization, tourmalinization and silicification. A mineralogical and geochemical zonation typical for granitic pegmatites has been identified that was affected by metasomatic/hydrothermal alteration, mainly albitization and greisenization. The latter alteration is associated with the main phase of cassiterite mineralization. A first stage with Nb–Ta, Li and minor Sn, however, already formed pre-alteration, directly associated with pegmatite crystallization. ^{40}Ar–^{39}Ar muscovite dating of unaltered pegmatites resulted in ages of 938.8 ± 5.1 Ma and 934.0 ± 5.9 Ma. These ages are overlapping with the U–Pb age of the Nb–Ta mineralization (940 ± 5.1 Ma), also giving new temporal constraints on the fertile E-group granite generation in the KIB. The ^{40}Ar–^{39}Ar muscovite age of a mineralized greisen is 923.3 ± 8.3 Ma, which is younger but still partly within error of the ^{40}Ar–^{39}Ar ages of the unaltered pegmatites. Based on the partial overlap in age, but also on field and paragenetic relationships and the stable isotope composition of the fluids, this greisenization and associated cassiterite mineralization can still be linked to the pegmatite crystallization.

© 2015 Elsevier B.V. All rights reserved.

1. Introduction

Manono-Kitotolo is located in the Central African Kibara belt, which forms together with the Karagwe-Ankole belt a Mesoproterozoic geological structure (Tack et al., 2010) that extends from the southern part of Katanga in the Democratic Republic of Congo (DRC) to the southwestern part of Uganda (Fig. 1; Cahen et al., 1984). The two belts are separated by a Rusizian basement rise that represents the NW extension across Lake Tanganyika of the Palaeoproterozoic Ubende belt (SW Tanzania). The Kibara belt (KIB) occurs in the Katanga province in the southwest of the DRC, while the Karagwe-Ankole belt (KAB) comprises Rwanda, Burundi, SW Uganda, northwestern Tanzania and the Kivu-Maniema region in the DRC (Fernandez-Alonso et al., 2012; Tack et al., 2010). The Kibara belt forms a belt of Palaeo- and Mesoproterozoic supracrustal units, mostly metasedimentary rocks with minor metavolcanic rocks, intruded by voluminous Mesoproterozoic "S-type" granitoid massifs and subordinate mafic bodies (Cahen et al., 1984; Kokonyangi et al., 2001, 2004, 2006). The Kibara and Karagwe-Ankole belts host a large metallogenic province that contains numerous granite-related ore deposits, with the typical metal association of Sn–W–Nb–Ta. The metals are dominantly present in pegmatites or quartz veins (e.g., Dewaele et al., 2011; Pohl et al., 2013). Pegmatites can be found mineralized with Nb–Ta minerals, cassiterite, amblygonite, spodumene, beryl, etc., while mineralized quartz veins mainly contain cassiterite or wolframite. During the last decade, renewed metallogenetic research on the Sn, W and Nb–Ta mineralization in the KAB and KIB has resulted in new insights in the formation of the granite related

* Corresponding author. Tel.: +32 (0) 2 769 5427; fax: +32 (0) 2 769 5432.
E-mail address: stijn.dewaele@africamuseum.be (S. Dewaele).

http://dx.doi.org/10.1016/j.oregeorev.2015.07.004
0169-1368/© 2015 Elsevier B.V. All rights reserved.

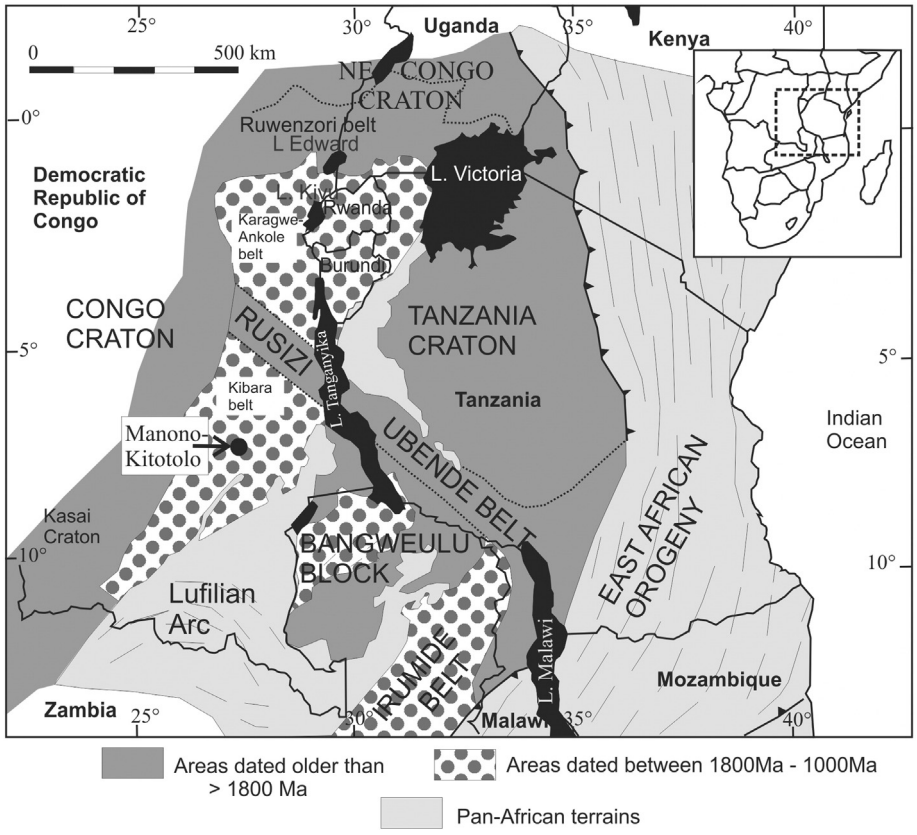

Fig. 1. Regional tectonic setting of the Kibara belt (KIB) and the Karagwe-Ankole belt (KAB) in Central Africa. Modified after Brinckmann et al. (2001).

mineralization in the Great Lakes area (e.g., Dewaele et al., 2011; Goldmann et al., 2013; Hulsbosch et al., 2013, 2014; Lehmann et al., 2014; Melcher et al., 2015; Pohl, 1994; Pohl and Günther, 1991; Pohl et al., 2013).

Manono-Kitotolo is a very large rare-metal pegmatite located in the northern part of the Katanga province of the Democratic Republic of Congo, ~500 km NW of Lubumbashi, which has mainly been exploited for cassiterite and columbite–tantalite (Bassot and Morio, 1989; Landa et al., 1950; Thoreau, 1950). The Manono-Kitotolo deposit consists of numerous open pit mines that extend over an area with a width of 800 m and that stretches over a distance of 15 km. From the start in 1915 until the stop of the exploitation in the mid 1980s, the deposit has produced about 140,000 tonnes of cassiterite concentrate and 4500 tonnes of columbite–tantalite concentrate (unpublished archives Géomines at the Royal Museum for Central Africa — RMCA). During the last decades of exploitation, the production continuously dropped not only due to technical problems, but also due to depletion of the altered and easily exploitable near-surface portions, resulting in an increasing importance of the unaltered pegmatite. The non-altered pegmatite is estimated to have a resource potential of about 200,000 tonnes of cassiterite and 10,000 tonnes of columbite–tantalite concentrate (unpublished archives Géomines, RMCA), which would make Manono-Kitotolo a world-class deposit. In addition, the spodumene potential has been evaluated during the beginning of the 1980s and has been estimated at 330,000 tonnes of Li (unpublished archives Géomines, RMCA), which would make it the fourth largest lithium pegmatite intrusion of the world. Prospection had also been carried out in the larger vicinity of the Manono-Kitotolo quarries (Laterite Kitotolo Nord, Flat Lukushi, etc.), where substantial reserves have been indicated. A borehole in the western part of the Kitotolo quarry has demonstrated that the mineralized pegmatite continues to a depth of at least 100 m, and is still open towards depth.

In this study, we focus on the geology and the timing of the formation of the primary Sn, Nb–Ta and Li mineralization of Manono-Kitotolo. This study of the Manono-Kitotolo deposit is largely based on unpublished geological information available in the mining archives of the companies that exploited the deposit in the past (Géomines, Zairétain and Congoétain; mining archives Royal Museum for Central Africa) and on the study of hundreds of rock and mineral concentrate samples present in the rock and mineral collection of the Royal Museum for Central Africa (RMCA). Due to logistical and security reasons, the Manono-Kitotolo has been largely inaccessible during the last decades. In addition, after the exploitation started, the main quarries have been flooded which complicates the study of the unaltered pegmatites.

2. Geology of the Kibara belt

The Karagwe-Ankole belt and the Kibara belt (Tack et al., 2010) of Central Africa formed and evolved between three pre-Mesoproterozoic domains: the Archaean–Palaeoproterozoic Congo Craton to the west and north, the Archaean Tanzania Craton to the east, and the Bangweulu Block to the south (Fig. 1). Two distinct segments are identified, separated in the Democratic Republic of the Congo (DRC) by the north-western extension of the Palaeoproterozoic Ubende belt (SW Tanzania) across Lake Tanganyika. The northern segment or Karagwe-Ankole belt (KAB: Rwanda, Burundi, Maniema and Kivu in the DRC) and southern segment or Kibara belt (KIB: Katanga in the DRC) are treated as two separate, but coeval belts (e.g., Tack et al., 2010).

The Mesoproterozoic Kibara fold belt (KIB) in Katanga consists dominantly of Palaeo- and Mesoproterozoic metasediments, covered by younger Neoproterozoic and Phanerozoic sedimentary rocks (Fig. 2; Laghmouch et al., 2012), that have been intruded by different generations of granitic and mafic rocks. Although the KIB has been intensely prospected during the last century, only the stratigraphy of the southern

part of the belt (south of 8°S) has been studied in detail, while the geology of the northern part (8°–5°S) is mainly known from remote sensing studies (ERTS, 1981). This study could only discriminate between the major litho-geomorphological units: Phanerozoic deposits, Neoproterozoic Bushimayian, undifferentiated Mesoproterozoic (Kibara), undifferentiated Palaeoproterozoic (Ruzizian) and "basement" consisting of undifferentiated units. The Palaeoproterozoic rocks of the Ruzizian Supergroup consist of (mica-) schists, (quartzo-) phyllites, quartzites, amphibolites, hornblendite–amphibolite schists, graphite-rich schists, phyllitic schists, meta-(?)arkoses and (migmatitic) gneisses (Cahen and Lepersonne, 1967). These Ruzizian rocks are mainly found in the northern part of the Kibara belt. Different stratigraphic successions have been established for the Mesoproterozoic rocks of the Kibara Supergroup (Cahen, 1954; Cahen and Lepersonne, 1967; Cahen et al., 1984), which have been compiled and combined by Laghmouch et al. (2012). The formal lithostratigraphy for the Kibara Supergroup comprises from bottom to top (Fig. 2): the Kiaora group, the Lufira (or Nzilo) Group, the Mount Hakansson Group and the Lubudi Group, each separated by an unconformity and/or a basal conglomerate. The Kiaora Group is estimated to be 1700 to 4300 m thick and is characterized by (quartzo-) phyllites and schists, with quartzitic horizons and with rhyolites at the top. The Lufira or Nzilo Group has a thickness between 2700 and 7000 m and is dominantly quartzitic, with locally (quartzo-) phyllitic levels and an important sequence of doleritic lavas and sills at the top. The Mount Hakansson Group is 1900 to 4000 m thick and contains dark-colored slates and quartzites. The Lubudi Group has a thickness of 600 to 1850 m and consists of dark-colored arkoses and conglomeratic lenses, black graphitic shale with sandstone levels and an upper part with limestones and dolomites.

The granitic intrusions in the Kibara fold belt have historically been subdivided into five groups (A to E) based on deformation degree and Rb–Sr dating (Cahen et al., 1984). Recent U–Pb SHRIMP dating indicates the presence of only two main granite generations in the KIB (Kokonyangi et al., 2001, 2004, 2006). The main granite generation A to D, which makes the majority of the granitic bodies on the geological map, has been dated at ~1381 ± 8 Ma (U–Pb SHRIMP zircon; Kokonyangi et al., 2001, 2004, 2006). The E-granites (or "tin granites") have not been age-dated by U–Pb SHRIMP in the KIB, but Rb–Sr ages of 977 ± 18 Ma (Mwanza Massif) and 966 ± 21 Ma (Mount Bia Massif) (Rb–Sr whole rock and mineral separates ages; Cahen and Ledent, 1979) have been proposed, based on the recalculation of data of Cahen et al. (1967, 1971). Intrusion of the E-granites is attributed to post-collisional relaxation after the main deformation phase resulting in the formation of the Kibara fold belt (Cahen et al., 1984; Kokonyangi et al., 2001, 2004, 2006). This E-granite generation has been interpreted as the parental granite for abundant pegmatites and quartz veins that can be mineralized with rare metals (Cahen and Ledent, 1979; Cahen et al., 1984) based on their non-deformed leucocratic appearance, similar age and spatial relationship with the mineralization. Several microcline, muscovite and lepidolite samples from different pegmatite locations in Katanga (Manono, Sofwe and Shienzi) have given a Rb–Sr age of 973 ± 13 Ma, which has been considered as the age of pegmatites in the KIB by Cahen and Ledent (1979), also based on the recalculation of the data of Cahen et al. (1967, 1971).

Numerous geodynamic models exist for the Mesoproterozoic KIB and KAB. These belts have been interpreted as: a collisional orogeny (Kampunzu et al., 1986; Kokonyangi et al., 2004, 2006; Rumvegeri, 1991), as an intracratonic orogen with different periods of extension and compression (Klerkx et al., 1984, 1987) and as an intracratonic extensional detachment structure, conditioned by transtensional strike-slip reactivation of NW-trending shear zones in the Palaeoproterozoic basement (Fernandez-Alonso and Theunissen, 1998). These models implicitly consider that the Kibaran orogeny occurred in Central Africa in late Mesoproterozoic times (1.4–1.0 Ga) and had a protracted character (Cahen et al., 1984). Kokonyangi et al. (2001, 2004, 2006) suggest that the A to D granites formed syn-deformational in a continental arc setting at ~1380 Ma. This D1 deformation is preserved as an ENE–WSW trending flow foliation S1 in the granitic rocks (Klerkx et al., 1984, 1987; Kokonyangi et al., 2001, 2004). In the metasedimentary rocks this S1 foliation is parallel to the S0 bedding. However, all granitic and metasedimentary rocks have been overprinted by a second deformation event (D_2), characterized by NW–SE trending isoclinal meso- and macroscale folds and reverse folds with associated S2 foliation, interpreted as the climax of the Kibaran orogeny (Kokonyangi et al., 2001, 2004, 2006). No age constraints are currently available for this main deformation event, but U–Pb SHRIMP dating of metamorphic zircon overgrowths in the Kisele monzogranite gneiss give an age of 1079 ± 14 Ma, which could be considered as a maximum age (Kokonyangi et al., 2004). This is largely consistent with a 1050 ± 50 Ma U–Pb yttrocrasite age in the Mandwe Granite gneiss (Ebenhardt et al., 1956) and a ~1030 Ma U–Pb zircon age in the Fwifwi leucomonzogranite (Cahen and Snelling, 1966).

However, Tack et al. (2010) have shown for the KAB that the prominent tectono-magmatic event is a short-lived intraplate transtensional anorogenic event at 1375 Ma related to the emplacement of a Large Igneous Province (LIP) with widespread granite and (ultra-)mafic intrusions. Compressional events occurred in the KAB at 1.0 Ga, as result of a far-field effect of the collisional Irumide and Chipata-Tete (or Southern Irumide) belts during Rodinia amalgamation (Johnson et al., 2005, 2007; De Waele et al., 2006, 2008, 2009). The morpho-structural response in the KAB (and the KIB) to the distant Irumide Orogen, was accommodated by displacement along the Ubende-Rusizi Belt (references in Fernandez-Alonso et al., 2012). In the KAB, the metasedimentary rocks were folded and thrusted as a result of reactivation of structures in the underlying Palaeoproterozoic basement (Theunissen, 1988, 1989) and developed a S2 foliation, postdating the S1-fabric which is related to the 1375 Ma Kibaran event (Tack et al., 2010). Post-compressional relaxation (i.e., post-S2) gave rise to the emplacement of the post-Kibaran Sn metallogenic province (new SHRIMP-age of tin-granite emplaced in the WD at ca. 986 Ma (Dewaele et al., 2011; Tack et al., 2010)). Subsequently during Gondwana amalgamation at 550 Ma, a second E to W directed compressional event affected the KAB as a far-field effect of the distant East African Orogen, giving rise to a pronounced squeezing of earlier structures, resulting in N–S trending thrust sheets and imbricate structures (Dewaele et al., 2011; Kabete et al., 2012; Rossetti et al., 2007).

3. Geological setting of the Manono-Kitotolo deposit

In the Manono-Kitotolo area, detailed regional geological studies are very limited. Ngulube (1994) observed two structural orientations, interpreted to represent two deformation events. Firstly, there is a S1 foliation parallel to the bedding S0, oriented N40–70°E in the metasediments and in the foliated and porphyritic granite of Manono. A second foliation S2, which is interpreted to be fold-related, is oriented NW and intersects the S1 foliation. The D2 deformation was not penetrative enough to obliterate the D1 structures. Therefore, the latter orientations define the structural orientations in the area. The rocks are also affected by a younger brittle fracturing, with diverse orientations. Based on the presence of S1 and S2, the rocks in the vicinity of Manono-Kitotolo can be attributed to the Kibara Supergroup (cf. Kokonyangi et al., 2004, 2006).

Three different types of granites have been identified in the Manono area by Ngulube (1994; Fig. 3). Firstly, there are the gray colored foliated and porphyritic granites (Lukushi, Kisudji and Pongo granite), which are characterized by the presence of both a S1 and S2 foliation. The granites are holocrystalline, inequigranular with phenocrysts of perthite, microcline, plagioclase and quartz, and with porphyroblasts of dominantly biotite and minor muscovite. In the Kisudji and Pongo granites, mineralized pegmatites are described that follow the S2 orientation. The second granite type is the migmatitic granite suite of Kazungu and Mukishi-Mukusuke. These granites are dark to light gray and show a

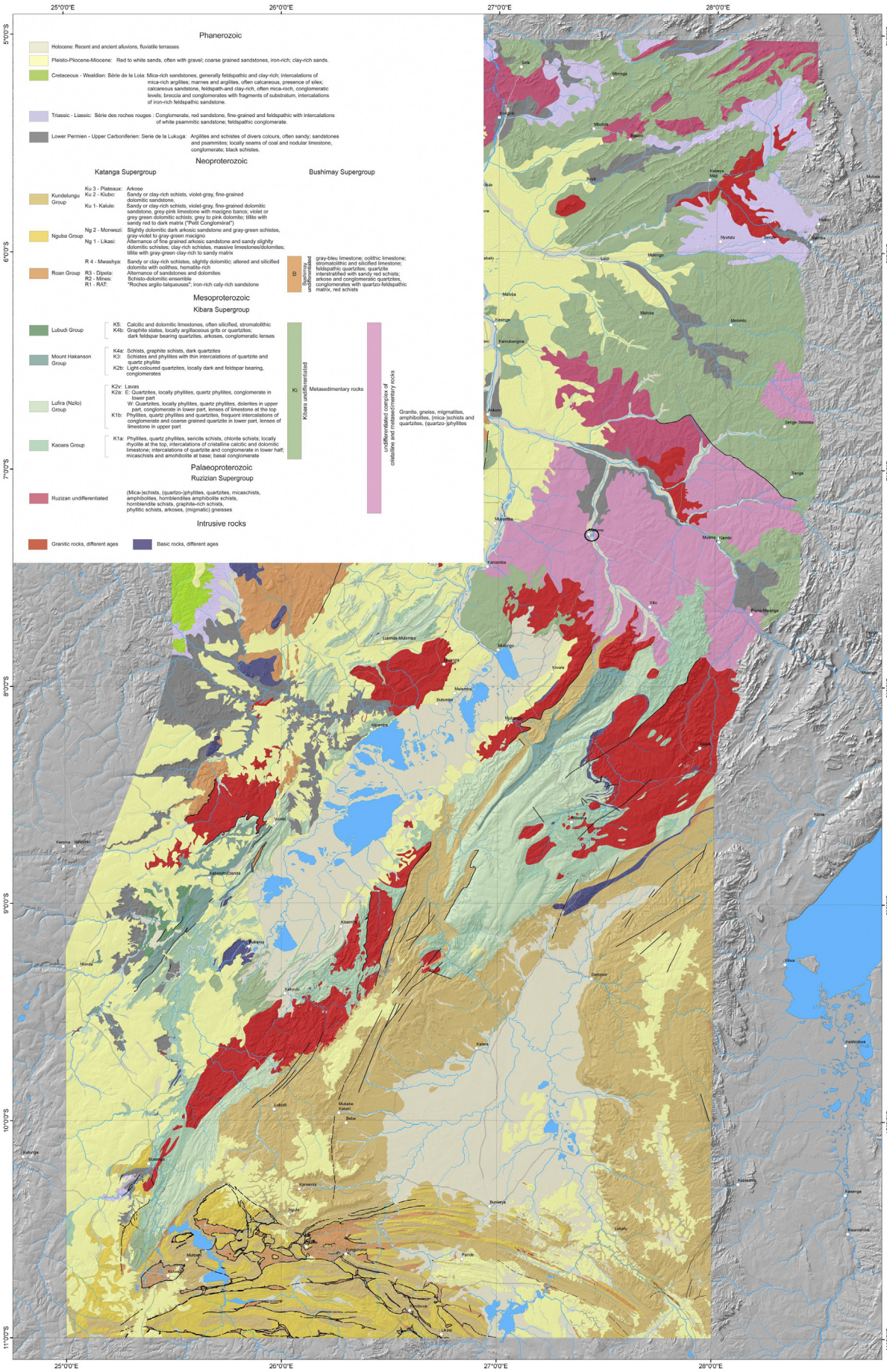
Phanerozoic
Holocene: Recent and ancient alluvions, fluviatile terrasses
Pleisto-Pliocene-Miocene: Red to white sands, often with gravel; coarse grained sandstones, iron-rich; clay-rich sands.
Cretaceous - Wealdian: Série de la Loia: Mica-rich sandstones, generally feldspathic and clay-rich; intercalations of mica-rich argilites; marnes and argilites, often calcareous, presence of silex; calcareous sandstone, feldspath-and clay-rich, often mica-roch, conglomeratic levels; breccia and conglomerates with fragments of substratum, intercalations of iron-rich feldspathic sandstone.
Triassic - Liassic: Série des roches rouges : Conglomerate, red sandstone, fine-grained and feldspathic with intercalations of white psammitic sandstone; feldspathic conglomerate.
Lower Permien - Upper Carboniferien: Serie de la Lukuga: Argilites and schistes of divers colours, often sandy; sandstones and psammites; locally seams of coal and nodular limestone, conglomerate; black schistes.
Neoproterozoic
Katanga Supergroup
Bushimay Supergroup
Kundelungu Group
Ku 3 - Plateaux: Arkose
Ku 2 - Kiubo: Sandy or clay-rich schists, violet-gray, fine-grained dolomitic sandstone,
Ku 1- Kalule: Sandy or clay-rich schists, violet-gray, fine-grained dolomitic sandstone, grey-pink limestone with macigno bancs; violet or grey green dolomitic schists; grey to pink dolomite; tillite with sandy red to dark matrix ("Petit Conglomérat")
Nguba Group
Ng 2 - Monwezi: Slightly dolomitic dark arkosic sandstone and gray-green schistes, gray-violet to gray-green macigno
Ng 1 - Likasi: Alternance of fine grained arkosic sandstone and sandy slightly dolomitic schistes; clay-rich schistes, massive limestones/dolomites; tillite with gray-green clay-rich to sandy matrix
Roan Group
R 4 - Mwashya: Sandy or clay-rich schistes, slightly dolomitic; altered and silicified dolomite with oolithes, hematite-rich
R3 - Dipeta: Alternance of sandstones and dolomites
R2 - Mines: Schisto-dolomitic ensemble
R1 - RAT: "Roches argilo-talqueuses", iron-rich caly-rich sandstone
B: gray-bleu limestone; oolithic limestone; stromatolithic and silicified limestone; feldspathic quartzites; quartzite interstratified with sandy red schists; arkose and conglomeratic quartzites, conglomerates with quartzo-feldspathic matrix, red schists
Mesoproterozoic
Kibara Supergroup
Lubudi Group
K5: Calcitic and dolomitic limestones, often silicified, stromatolithic
K4b: Graphito slates, locally argillaceous grits or quartzites; dark feldspar bearing quartzites, arkoses, conglomeratic lenses
Mount Hakanson Group
K4a: Schists, graphite schists, dark quartzites
K3: Schistes and phyllites with thin intercalations of quartzite and quartz phyllite
K2b: Light-coloured quartzites, locally dark and feldspar bearing, conglomerates
Lufira (Nzilo) Group
K2v: Lavas
K2a: E: Quartzites, locally phyllites, quartz phyllites, conglomerate in lower part
W: Quartzites, locally phyllites, quartz phyllites, dolerites in upper part, conglomerate in lower part, lenses of limestone at the top
K1b: Phyllites, quartz phyllites and quartzites, frequent intercalations of conglomerate and coarse grained quartzite in lower part, lenses of limestone in upper part
Kaoara Group
K1a: Phyllites, quartz phyllites, sericite schists, chlorite schists; locally rhyolite at the top, intercalations of cristalline calcitic and dolomitic limestone; intercalations of quartzite and conglomerate in lower half; micaschists and amohibolite at base; basal conglomerate
Ki: Kibara undifferentiated: Metasedimentary rocks
undifferentiated complex of cristalline and metasedimentary rocks: Granito, gneiss, migmatites, amphibolites, (mica-)schists and quartzites, (quartzo-)phyllites
Palaeoproterozoic
Ruzizian Supergroup
Ruzizan undifferentiated: (Mica-)schists, (quartzo-)phyllites, quartzites, micaschists, amphibolites, hornblendites amphibolite schists, hornblendite schists, graphite-rich schists, phyllitic schists, arkoses, (migmatic) gneisses
Intrusive rocks
Granitic rocks, different ages
Basic rocks, different ages
25°0'0"E
26°0'0"E
27°0'0"E
28°0'0"E
5°0'0"S
6°0'0"S
7°0'0"S
8°0'0"S
9°0'0"S
10°0'0"S
11°0'0"S

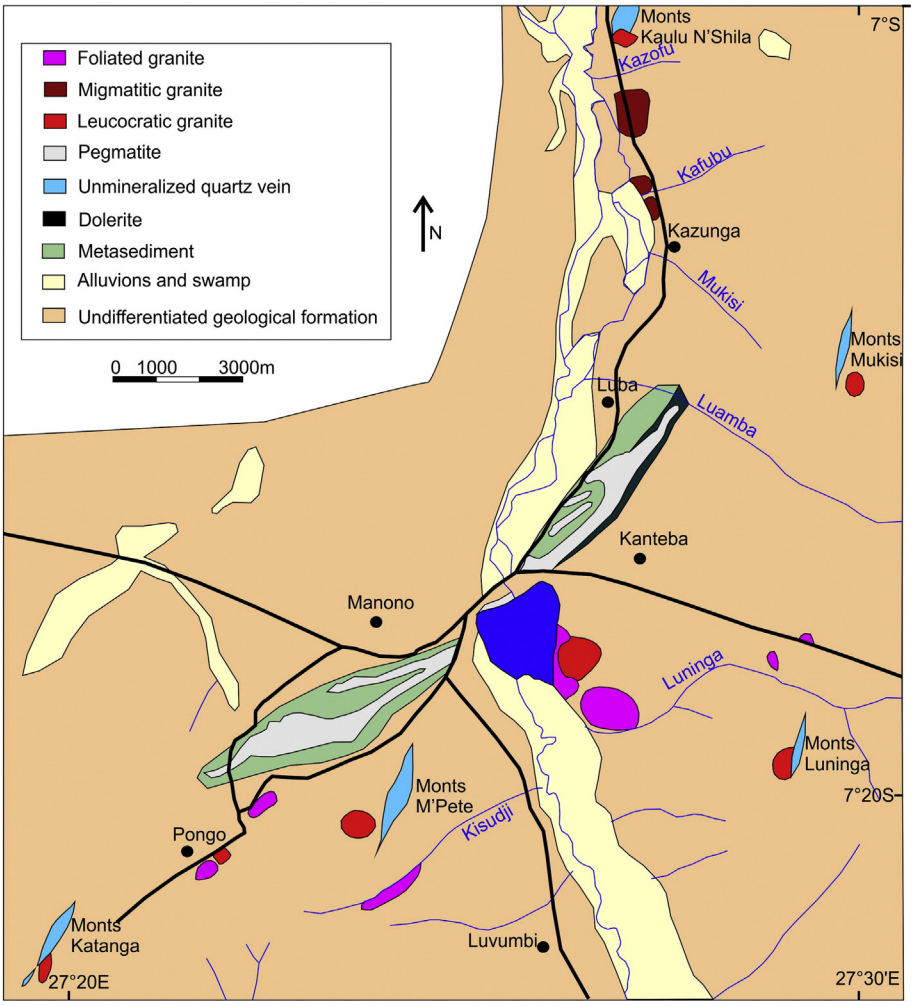

Fig. 3. Detailed geological map of the larger Manono-Kitotolo area.
Modified after Ngulube (1994).

subequigranular migmatitic to (sub-) porphyric texture. Different foliation directions have been identified in these granites. The granites are holocrystalline, hypidiomorphic, slightly inequigranular with euhedral microcline, perthite or plagioclase minerals in a matrix of quartz, plagioclase, perthite, biotite and little muscovite. These migmatitic granites are often crosscut by barren quartz veins and cassiterite-mineralized small pegmatite veins. The third group of granites (Lukushi and M'Pete leucogranite) is characterized by reddish, equigranular, hypidiomorphic leucocratic crystal textures. They consist of quartz, microcline, plagioclase, perthite, muscovite and biotite together with abundant tourmaline, garnet, and little chlorite or sericite. No foliation can be identified in this granite type. At Lukushi, it can be observed that the leucogranites also crosscut the foliated and porphyric granites. At this contact the leucogranite can have an aplitic structure. They often contain miarolitic cavities that are filled with minerals like muscovite, and tourmaline. The latter granites occur as small stocks in the immediate vicinity of the Manono-Kitotolo quarry. No crosscutting quartz veins and pegmatites are identified in these leucogranites. Mineralized pegmatitic zones have been identified in the upper parts of these granites. Based on the lack of cross-cutting foliation and the leucocratic texture in this third group of granites, they are interpreted to have intruded post-deformation and could be identified as E-type granites (Cahen et al., 1984).

The Manono-Kitotolo deposit (Fig. 4A and B) consists of two main zones that stretch over an area with a length of ~15 km and a width of ~800 m: Kitotolo in the southwest and Manono-Kahungwe in the northeast (Landa et al., 1950; Thoreau, 1950). The two exploited zones are separated at a distance of 2 km by the artificial Lake Lukushi, where, granite and spodumene-bearing pegmatites are exposed (Bassot and Morio, 1989). In the Kitotolo sector, the pegmatites occur in phyllitic or schistose rocks with some meta-sandstone levels, while they crosscut metadoleritic rocks in the Manono-Kahungwe sector. The general structural orientation in the metasedimentary rocks is N30–60E (unpublished data mining archives RMCA), which has been interpreted as the S1/S0 orientation. The dip of the bedding can vary between 50°S to sub-vertical. Both sectors contain different individual pegmatite veins separated by metasedimentary or metadoleritic segments (Fig. 5A, B). The intruded pegmatites have a general orientation of N40–60E and dips varying between 50°N to 50°S, but predominantly subvertical (unpublished data mining archives RMCA). The contact with the metasedimentary rocks shows some small-scale folding due to the intrusion of the pegmatites. The contact is, however, largely parallel to the regional foliation orientation and the pegmatites are interpreted to have intruded along the existing foliation planes. The individual pegmatite veins have been affected by important post-emplacement fracturing, which often resulted in complex displacements between blocks.

Fig. 2. Geological map of the Kibara belt and the surrounding Precambrian area, Katanga, Democratic Republic of Congo (Laghmouch et al., 2012). The location of Manono-Kitotolo is indicated by the circle.

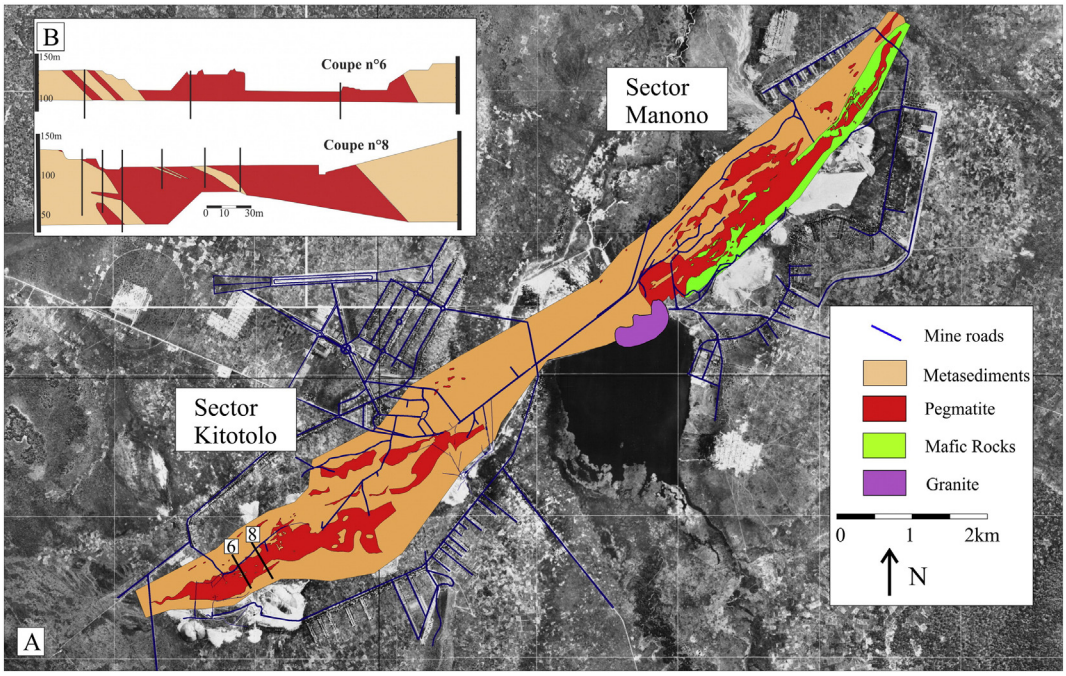

Fig. 4. A. Detailed geological map of the pegmatites in the Manono-Kitotolo quarries, based on unpublished archives of Géomines (RMCA). B. Simplified cross-sections through the Kitotolo zone, indicating the presence of different pegmatite bodies crosscutting metasediments. Location of the cross-sections is indicated on figure A.
Based on unpublished archives of Géomines (RMCA).

Superficial weathering resulted in the alteration of the pegmatite. The average thickness of the eluvial cover is ~8 m and consists either of brownish sandy or clayey–sandy, loose laterites, crumbly laterites or even hard laterites. This weathering can extend to a depth of 80 m in the Manono sector and obscures the identification of the mineralogy, structure and zonation of the primary pegmatites. It should be mentioned that in boreholes in the Kitotolo quarry, mineralized pegmatite has been found to a depth of at least 100 m, and the deposit is still open towards depth. Based on this vertical continuity, the exceptional dimension of the Manono-Kitotolo pegmatites and the regional mineralogical homogeneity, Bassot and Morio (1989) concluded that the pegmatites form part of a granitic cupola system and are located in the upper part of the parental granite. They considered that Manono-Kitololo formed by the crystallization from residual magmatic fluids in the upper part of an upwardly differentiated granitic pluton. It occurs as a sheet-like pegmatite with disseminated mineralization in the cupola of the granite system (cf Variscan Sn mineralization in France and Germany; Černý et al., 2005). However, this model has been questioned by Dill (2015) who states that Manono-Kitololo pegmatites exhibit unidirectional growth zones from bottom to top, which makes it hard to accept that a parallel injection took place for the entire dimension of the Manono-Kitotolo pegmatites.

4. Petrography and paragenesis of the Manono-Kitotolo pegmatites

The intrusion of the different pegmatite bodies in metasedimentary rocks and metadolerites at Manono-Kitotolo resulted in an intense alteration of limited width, which is typically identified by the increase

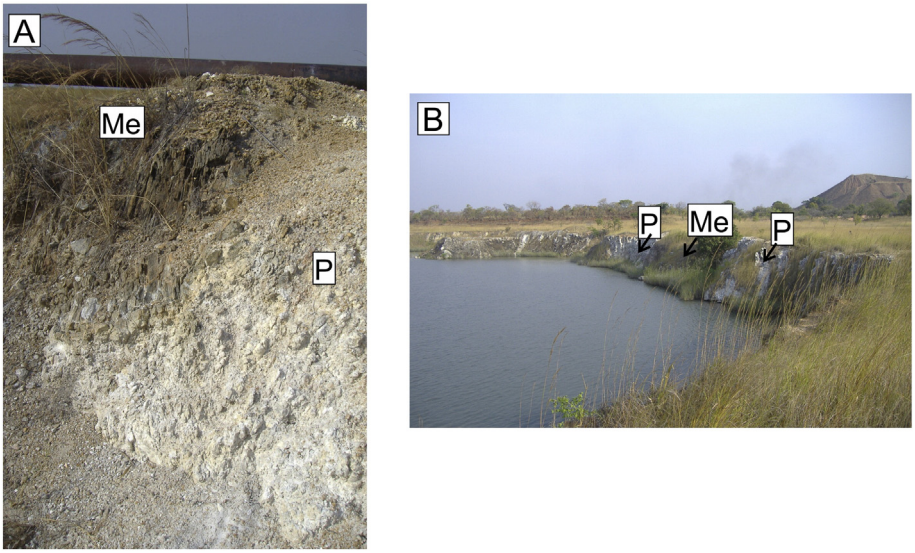

Fig. 5. A. Contact between pegmatite (P) and metasedimentary rocks (Me), with high-angle foliation. B. Different pegmatite veins (P) cross-cutting metasedimentary rocks (Me).

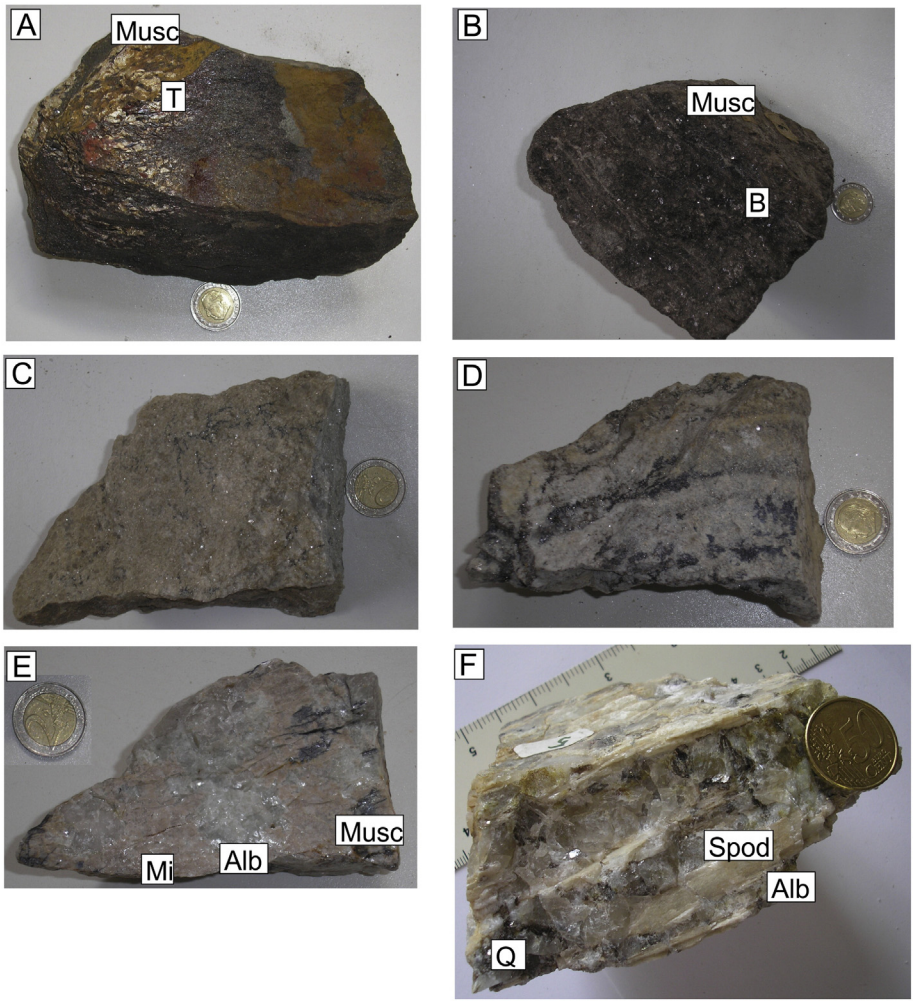

Fig. 6. A. Altered host-rock with tourmaline (T) and muscovite (Musc). B. Altered host-rock with biotite (B) and muscovite (Musc). C. Fine-grained border zone of pegmatite, with quartz, microcline, albite and micas. D. Fine-grained wall zone of pegmatite consisting of quartz, microcline, albite and micas. E. Intermediate zone of pegmatite with microcline (Mi), albite (Alb) and muscovite (Musc). F. Intermediate zone of pegmatite with spodumene (Spod), albite (Alb) and quartz (Q).

of tourmaline (Fig. 6A). The metadolerites are fine-grained and are often crosscut by small quartz veinlets. Microscopically, they dominantly consist of quartz with little feldspar, biotite, tourmaline, muscovite and iron oxides. The metadolerites can be completely recrystallized to a biotite-rich rock. This biotite has often been strongly influenced by retrograde chloritization. The metasedimentary host-rocks are mainly micaschists or phyllites, which show a well-developed foliation. These rocks dominantly consist of quartz, tourmaline, muscovite and/or biotite (Fig. 6A and B), but often staurolite and iron oxides can be identified. The latter minerals often formed parallel to the foliation orientation.

Internal zonation, typically observed in granitic pegmatite dikes (Cerny, 1991; London, 2014), is obscured by the lack of colored minerals, the degree of weathering and the dimension and orientation of pegmatite veins (Bassot and Morio, 1989). The study of the zonation of the primary pegmatites is further complicated since the quarries have been flooded after the termination of the industrial exploitation about 30 years ago. Although the exact location of the studied samples is unknown, it is attempted to position the different samples in the typical zonation scheme of pegmatites (Cameron et al., 1949; London, 2008, 2014) based on their mineralogical composition, grain size and morphology. Based on this theoretical classification, the pegmatite samples can be divided into a border zone, a wall zone, an intermediate zone and the core. This not necessarily implies that all these zones are always present and well-developed. However, for the ease of the description we will use the general zonal terms described in the literature (Cameron et al., 1949; London, 2008, 2014). A zonation has been described at Manono-Kitotolo (Bassot and Morio, 1989; Landa et al., 1950; Ngulube, 1994; Thoreau, 1950) in the past and observed in hand specimens in this study.

The border zone is formed by a fine-grained millimeter-scale mass with a granitic texture, and is mainly composed of quartz, muscovite, microcline and albite (Fig. 6C). Some isolated grains of green-colored beryl can be identified. This border zone is identified in samples that contain parts of the host-rock, indicating that the samples define the pegmatite-hostrock margin. They are historically been called “aplite albitique” (Landa et al., 1950; Thoreau, 1950). The next zone inwards, “the wall zone”, consists of coarser grained quartz, microcline, albite and micas (Fig. 6D). Again some beryl has been identified. The mineralogy is identical to the border zone, but the grain size of the minerals is coarser, but still millimeter-size. Both columbite–tantalite and cassiterite can be found in samples from the wall zone. Since the border zone is in general only some centimeters thick, the wall zone can be studied in the same samples. The intermediate zone is characterized by a large increase in crystal size and contains quartz, spodumene, petalite, microcline, albite and micas (Fig. 6E and F). Different mineralogical subtypes can be identified in the intermediate zone based on the dominant mineral present. The K-feldspar subzone consists dominantly of orthoclase and microcline, with little albite, quartz and muscovite. The relative

abundance of orthoclase and microcline can vary largely. Columbite–tantalite and cassiterite crystals have been identified in samples from this subzone. In the spodumene subzone, the main minerals are quartz and spodumene, with minor amounts of K-feldspar, muscovite, apatite and opaque minerals (iron oxides, columbite–tantalite and cassiterite). The spodumene crystals often have different colors (green, pink, beige), are often fractured and associated with muscovite. The latter subzone is historically called the zone of "pegmatites à colonnes" (Landa et al., 1950; Thoreau, 1950), due to the large, prismatic spodumene crystals (Figs. 6F, 7A). In the albite subzone, the dominant mineral is albite with minor quartz. Cassiterite has been identified in these rocks. The albite crystals in these rocks have a larger centimeter to decameter crystal size compared to the cleavelandite and saccharoidal albite of the later albitization. However, the rocks in the albite subzone have also been submitted to later albitization and greisenization. The albite-spodumene subzone consists predominantly of albite, with spodumene, quartz, and little muscovite. Columbite–tantalite mineralization is identified in these rocks. The quartz subzone consists dominantly of quartz and lepidolite, and little spodumene and albite. A typical monomineralic quartz zone (Cameron et al., 1949; London, 2008, 2014) has not been identified and has not been described in the literature (Landa et al., 1950; Thoreau, 1950). Norton (1983) described a pegmatite core that is essentially made of lepidolite, plagioclase, quartz and microcline. Samples with such a mineralogical composition have been identified at Manono-Kitotolo and could be considered as core zone of the pegmatites (cf. Ngulube, 1994).

The primary mineralogy of the different pegmatite zones has been submitted to an intense alteration, dominantly albitization followed by greisenization. The intensity of albitization can vary largely throughout the pegmatitic bodies. In some samples, the primary pegmatite mineralogy with e.g., orthoclase (Fig. 7B) and spodumene can still be observed, while in other samples they are completely overprinted and only some quartz remains in the albitized rock (Fig. 7C). During the first stage of albitization, saccharoidal albite formed, which is preceded by the formation of cleavelandite. Rutile, cassiterite and columbite–tantalite seem to predate the albitization. The second important alteration phase is muscovitization (the so-called "poches de greisen"). The pegmatitic rocks have been altered to a mixture of centimeter-size quartz, muscovite and cassiterite (Fig. 7D). This process of greisenization is often not fully pervasive and primary feldspar minerals can still be identified. Not all greisen samples are mineralized. The cassiterite which precipitated during greisenization has a larger grain size – often with crystals of cm size – than the cassiterite formed prior to the alteration. Columbite–tantalite seems not to be associated with the greisenization.

The columbite–tantalite and cassiterite mineralization in the Manono-Kitotolo pegmatite has been observed in the unaltered border and intermediate zone of the pegmatite, where they occur as disseminated minerals. Columbite–tantalite clearly formed prior to the metasomatic alteration. Columbite–tantalite is the major carrier of Nb and Ta, with minor thoreaulite, wodginite and tapiolite and other Nb–Ta minerals present (e.g., Buttgenbach, 1933; Kristiansen, 2001). Cassiterite is much less abundant in pegmatitic rocks that have not been affected by the metasomatic alteration. The largest cassiterite crystals and the highest concentrations are found in the greisenized samples. Columbite–tantalite and cassiterite can be found in albitized samples (Fig. 7C), but there is no petrographic indication that these minerals precipitated during the albitization. They are, therefore, considered as remnants of the primary unaltered pegmatite composition. Nb–Ta minerals represent in general 5–10% of the cassiterite concentrates (unpublished archives Géomines, RMCA).

Spodumene clearly formed prior to the metasomatic alteration. The relative proportion of spodumene in certain zones of the pegmatite can reach 25%. The supergene alteration of spodumene often resulted in the reduction of the Li-concentration (Aderca, 1950; Thoreau, 1950). Accessory minerals that have been described for the Manono-Kitotolo

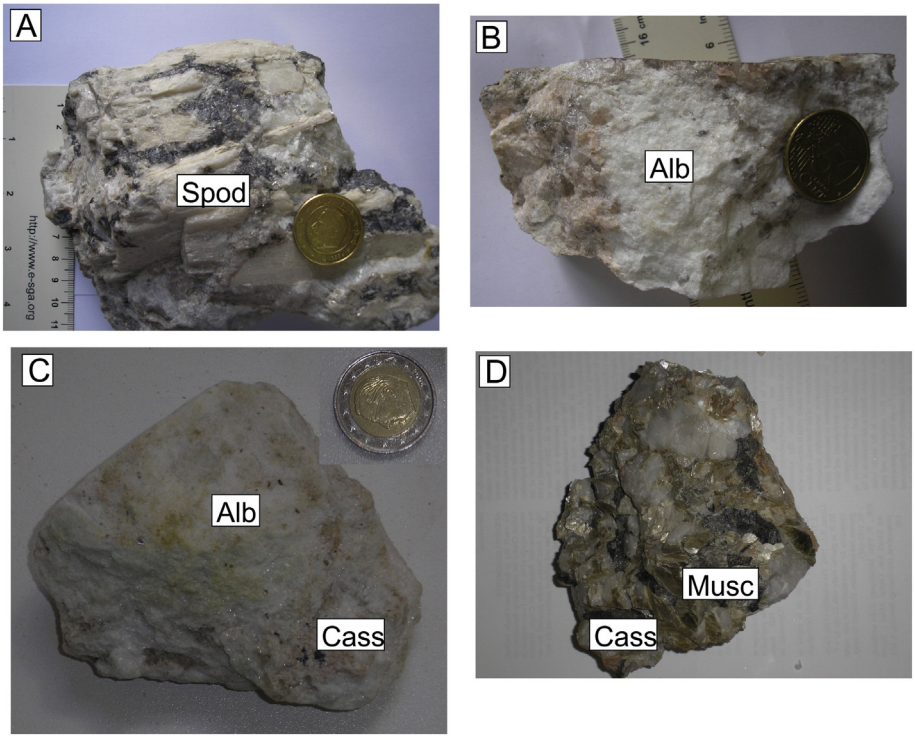

Fig. 7. A. Spodumene (Spod) in pegmatite. B. Partly albitized zone (Alb) in pegmatite. C. Albitized zone (Alb) in pegmatite with cassiterite (Cass). D. Greisenized zone in pegmatite with large crystals of muscovite (Musc), cassiterite (Cass) and quartz (Q).

Table 1
Major element composition of mica varieties collected from the internal zone of the Manono-Kitotolo pegmatites. Detailed description of the different muscovite and lepidolite samples in association with the identified internal pegmatites zones and alteration assemblages is given in the text.

Nr.	1	2	3	4	5	6	7	8	9	10	11	12	13	14
Sample	RG 16811	RG 16729	RG 5826	RG 9699	RG 15992	RG 16005	RG 8337	RG 8337	RG 3113	RG 16727	RG 16747	RG 16777	RG 16958	RG 16775
Subzone	Border	Wall	Intermediate: K-feldspar	Intermediate: K-feldspar	Intermediate: spodumene	Intermediate: albite–spodumene	Intermediate: K-feldspar	Intermediate: K-feldspar	Border	Wall	Cassiterite greisen	Cassiterite greisen	Barren greisen	Quartz
Metasomatism	/	/	/	/	/	/	Albitization	Albitization	Greisenization	Greisenization	Greisenization	Greisenization	Greisenization	/
Composition[a]	Muscovite	Muscovite	Muscovite	Muscovite	Muscovite	Muscovite	Muscovite	Muscovite	Muscovite	Muscovite	Muscovite	Muscovite	Muscovite	Lepidolite
SiO_2 (wt.%)	47.89	46.87	46.56	47.53	47.46	46.90	49.97	49.43	46.79	47.25	58.64	46.44	45.81	55.47
TiO_2	0.03	0.01	0.26	0.03	0.03	0.04	0.04	0.04	0.05	0.03	0.04	0.03	0.02	0.01
Al_2O_3	35.80	35.89	33.60	33.49	34.73	33.70	32.99	32.56	37.14	33.57	28.12	34.82	37.40	25.65
FeO_T	1.23	0.82	4.03	2.27	1.73	2.97	2.38	2.34	0.78	2.70	1.15	1.58	0.66	0.04
MnO	0.04	0.03	0.05	0.27	0.30	0.27	0.19	0.18	0.06	0.36	0.12	0.20	0.16	0.39
MgO	0.24	0.13	0.61	0.06	0.04	0.04	0.09	0.09	0.10	0.03	0.06	0.10	0.05	0.03
CaO	0.01	0.53	0.01	0.01	0.17	0.09	0.02	0.02	0.01	0.01	0.01	<0.01	<0.01	<0.01
Li_2O[b]	0.17	0.05	0.05	0.58	0.18	0.49	0.11	0.11	0.57	0.61	0.23	0.52	0.20	3.75
Na_2O	1.08	1.15	0.48	0.54	0.92	0.62	1.32	1.30	0.93	0.56	0.52	0.66	0.75	0.37
K_2O	9.37	9.16	10.66	10.13	9.85	10.32	9.15	8.93	9.72	10.20	7.96	9.91	10.17	9.02
P_2O_5	0.03	0.39	0.02	0.03	0.16	0.10	0.04	0.03	0.03	0.02	0.03	0.04	0.05	0.03
F	0.54	0.22	0.21	n.d.	0.56	1.19	0.37	0.37	n.d.	n.d.	0.68	1.24	0.61	4.05
Cl	0.00	0.00	0.00	n.d.	0.01	0.01	0.01	0.01	n.d.	n.d.	0.01	0.00	0.01	0.02
H_2O[c]	4.32	4.42	4.39	4.49	4.26	3.92	4.40	4.35	4.59	4.50	4.43	3.89	4.25	2.67
O=F,Cl	0.23	0.09	0.09	0.00	0.24	0.50	0.16	0.16	0.00	0.00	0.29	0.52	0.26	1.71
Total	100.56	99.59	100.84	99.44	100.16	100.16	100.90	99.60	100.77	99.84	101.71	98.91	99.87	99.79
Structural formula on the basis of 22 O atoms														
Si	6.27	6.22	6.22	6.34	6.29	6.27	6.54	6.55	6.11	6.30	7.40	6.21	6.06	7.24
Al (IV)	1.73	1.78	1.78	1.66	1.71	1.73	1.46	1.45	1.89	1.70	0.60	1.79	1.94	0.76
(Z)	8.00	8.00	8.00	8.00	8.00	8.00	8.00	8.00	8.00	8.00	8.00	8.00	8.00	8.00
Al (VI)	3.80	3.83	3.51	3.61	3.71	3.57	3.63	3.63	3.82	3.58	3.58	3.71	3.88	3.19
Ti	0.00	0.00	0.03	0.00	0.00	0.00	0.00	0.00	0.01	0.00	0.00	0.00	0.00	0.00
Fe^{2+}_T	0.13	0.09	0.45	0.25	0.19	0.33	0.26	0.26	0.09	0.30	0.12	0.18	0.07	0.00
Mn	0.00	0.00	0.01	0.03	0.03	0.03	0.02	0.02	0.01	0.04	0.01	0.02	0.02	0.04
Mg	0.05	0.03	0.12	0.01	0.01	0.01	0.02	0.02	0.02	0.01	0.01	0.02	0.01	0.01
Li	0.09	0.03	0.03	0.31	0.10	0.27	0.06	0.06	0.30	0.33	0.12	0.28	0.11	1.32
(Y)	4.08	3.98	4.14	4.22	4.05	4.21	3.99	3.99	4.23	4.26	3.85	4.21	4.09	4.56
Ca	0.00	0.07	0.00	0.00	0.02	0.01	0.00	0.00	0.00	0.00	0.00	0.01	0.01	0.01
Na	0.28	0.30	0.13	0.14	0.24	0.16	0.33	0.33	0.23	0.15	0.13	0.17	0.19	0.09
K	1.57	1.55	1.82	1.72	1.66	1.76	1.53	1.51	1.62	1.74	1.28	1.69	1.71	1.50
Rb	0.02	0.02	0.03	0.04	0.05	0.05	0.03	0.04	0.04	0.04	0.04	0.05	0.05	0.13
Cs	0.00	0.00	0.00	0.00	0.00	0.00	0.00	0.00	0.00	0.00	0.00	0.00	0.00	0.01
(X)	1.86	1.94	1.97	1.91	1.98	1.98	1.90	1.88	1.90	1.93	1.45	1.93	1.97	1.75
OH	3.78	3.91	3.91	4.00	3.76	3.50	3.85	3.84	4.00	4.00	3.73	3.47	3.74	2.33
F	0.22	0.09	0.09	0.00	0.23	0.50	0.15	0.16	0.00	0.00	0.27	0.52	0.25	1.67
Cl	0.00	0.00	0.00	0.00	0.00	0.00	0.00	0.00	0.00	0.00	0.00	0.00	0.00	0.00
feal[a]	−3.65	−3.73	−3.02	−3.32	−3.48	−3.21	−3.34	−3.35	−3.72	−3.23	−3.44	−3.51	−3.79	−2.98
mgli[a]	−0.04	0.00	0.10	−0.30	−0.09	−0.26	−0.04	−0.04	−0.28	−0.32	−0.11	−0.26	−0.10	−1.93

[a] Composition of mica varieties based on feal = octahedral ($Fe_T + Mn + Ti - Al^{VI}$) versus mgli = octahedral (Mg–Li); Tischendorf et al. (2001).
[b] Calculated from Li–F and Li–Rb_2O relationships of Tischendorf et al. (1997).
[c] Calculated from stoichiometric considerations; Tindle and Webb (1990).

Table 2
Trace element composition of mica varieties collected from the internal zone of the Manono-Kitotolo pegmatites. Detailed description of the different muscovite and lepidolite samples in association with the identified internal pegmatites zones and alteration assemblages is given in the text.

Nr.	1	2	3	4	5	6	7	8	9	10	11	12	13	14
Sample	RG 16811	RG 16729	RG 5826	RG 9699	RG 15992	RG 16005	RG 8337	RG 8337	RG 3113	RG 16727	RG 16747	RG 16777	RG 16958	RG 16775
Subzone	Border	Wall	Intermediate: K-feldspar	Intermediate: K-feldspar	Intermediate: spodumene	Intermediate: albite–spodumene	Intermediate: K-feldspar	Intermediate: K-feldspar	Border	Wall	Cassiterite greisen	Cassiterite greisen	Barren greisen	Quartz
Metasomatism	/	/	/	/	/	/	Albitization	Albitization	Greisenization	Greisenization	Greisenization	Greisenization	Greisenization	Greisenization
Composition*	Muscovite	Muscovite	Muscovite	Muscovite	Muscovite	Muscovite	Muscovite	Muscovite	Muscovite	Muscovite	Lithian muscovite	Muscovite	Muscovite	Lepidolite
Cr	1.3	0.9	1.3	2.3	5.1	4.5	6.6	6.7	3.8	1.3	5.2	0.6	1.3	1.3
Co	0.86	<0.40	0.90	<0.40	<0.40	<0.40	0.95	0.93	0.76	<0.40	0.75	<0.40	<0.40	<0.40
Ni	2.6	1.7	1.4	1.4	3.2	3.4	3.9	4.8	2.0	4.5	3.4	1.0	1.6	1.2
Cu	10	6.7	4	21	13	2	25	29	14	44	<1.8	<1.8	2.1	2.2
Zn	92	87	202	576	548	584	418	414	185	849	340	839	331	184
Ga	76	72	209	133	148	165	121	121	115	120	123	114	122	123
Ge	6.2	6.3	3.0	7.2	7.6	7.4	6.9	6.5	6.6	6.8	6.6	6.5	7.1	17.4
Rb	1954	2322	2747	4561	5415	5242	3774	3819	4503	4762	4159	5776	5810	14,573
Sr	43	57.9	4.5	1.2	14.0	3.1	1.6	1.7	13	0.85	0.71	0.35	1.2	0.22
Y	6.20	0.62	1.16	0.72	0.16	0.13	0.33	0.35	1.84	0.22	0.07	0.25	0.10	0.29
Zr	10.2	<0.09	8.1	0.2	164	0.9	4.7	5.4	3.7	10.6	<0.09	<0.09	<0.09	10.0
Nb	95	84	489	189	153	230	196	195	57	131	141	113	83	97
Sn	501	377	73	702	733	768	673	651	611	685	1633	794	916	323
Cs	100	151	91	386	370	367	230	231	256	383	238	597	297	2511
Ba	426	321	75	14	16	6	44	45	64	16	3	5	13	11
La	2.17	<0.01	0.05	<0.01	<0.01	<0.01	<0.01	<0.01	0.60	<0.01	<0.01	<0.01	<0.01	<0.01
Ce	5.25	0.43	1.68	0.13	0.06	0.02	0.36	0.34	2.26	0.09	<0.01	0.12	0.06	<0.01
Pr	0.82	0.07	0.17	0.04	0.02	0.02	0.05	0.05	0.25	0.04	<0.01	0.02	<0.01	<0.01
Nd	3.77	0.29	0.72	0.23	0.07	0.03	0.24	0.23	0.98	0.21	<0.01	0.05	0.02	0.03
Eu	0.26	0.87	0.02	0.02	<0.01	0.02	0.04	0.04	0.06	0.02	<0.01	<0.01	<0.01	<0.01
Sm	0.92	0.08	0.31	0.08	0.01	0.01	0.06	0.07	0.26	0.06	<0.01	0.02	<0.01	0.02
Gd	0.99	0.08	0.25	0.07	0.03	<0.01	0.07	0.07	0.22	0.03	<0.01	0.03	0.01	0.02
Dy	0.98	0.11	0.22	0.08	0.02	0.04	0.06	0.06	0.32	0.05	0.01	0.04	0.02	0.04
Ho	0.36	0.02	0.03	0.02	<0.01	0.02	0.01	0.01	0.06	0.02	<0.01	0.01	<0.01	0.01
Er	0.56	0.05	0.09	0.05	0.01	0.02	0.03	0.03	0.17	0.03	<0.01	0.01	<0.01	0.03
Yb	0.48	0.05	0.09	0.03	0.05	0.03	0.02	0.02	0.17	0.02	<0.01	0.01	<0.01	0.03
Lu	<0.01	<0.01	<0.01	<0.01	<0.01	<0.01	<0.01	<0.01	<0.01	<0.01	<0.01	<0.01	<0.01	<0.01
Hf	1.2	0.23	1.2	0.28	14	0.27	0.84	0.68	0.29	0.45	0.22	0.14	0.10	0.83
Ta	125	103	38	70	122	70	121	117	79	48	66	55	41	194
W	13.0	12.2	4.5	36.9	20.7	34.5	27.7	28.2	6.5	29.6	11.5	14.2	7.9	17.2
Pb	31	33	3.4	8.4	8.3	6.4	13.8	11.2	15.4	6.4	3.7	3.5	5.8	7.5
Th	2.78	1.04	1.01	0.07	6.1	0.57	0.95	0.92	0.94	0.71	1.01	0.11	0.07	0.27
U	2.2	1.77	0.21	0.43	10	0.89	2.0	2.0	0.40	0.75	0.14	0.10	0.13	0.19

pegmatites (Aderca, 1950, Bassot and Morio, 1989; Thoreau, 1950), but not identified during this study, are fluorite, zircon, thoreaulite, arsenopyrite, pyrite, ilmenite and traces of autunite (or uranocircite).

5. Mineral geochemistry

5.1. Mica compositional data

The composition of micas associated with different assemblages of the internal pegmatite zonation at Manono-Kitotolo have been analyzed by inductively coupled plasma optical emission (ICP-OES) at the division of Geology (KU Leuven) for their major elements (Table 1) and by mass spectrometry (ICP-MS) at the geochemistry department (RMCA) for their trace element composition (Table 2). Muscovite sheets have been microscopically hand-picked, powdered and dissolved by an adapted lithium metaborate flux procedure, with the exception for the Li-analyses. The latter have been calculated based on the known relationships with the mica's Rb_2O and F content (Tischendorf et al., 1997). Detailed sample preparation, analytical and standardization procedures, together with obtained analytical precision and accuracy, of the OES and MS analyses are given in Hulsbosch et al. (2014). Halogen (F and Cl) analyses of micas have been performed by ion chromatography (Table 1). Halogens were extracted from powdered mica samples using the pyrohydrolysis technique described by Balcone-Boissard et al. (2009; and references therein). Powdered sample (100 mg) was mixed with V_2O_5 (300 mg) and placed in a ceramic crucible. The sample was directly introduced into a quartz combustion tube and heated at 1100 °C through a H_2O-vapor stream. The halogen-containing (as halogen acids) H_2O-vapor by hydrolysis was condensed via a cooling system and trapped in a vial containing a 10 ml NaOH solution. After the extraction, F and Cl anions were determined by liquid chromatography using a Dionex ICS 2000 ion chromatograph with an Ion Pac AS18 (Dionex) anionic column. Fluoride and chloride standard solutions were used for ion chromatography calibration. Reported detection limits in rock samples were ~20 ppm for both elements (Balcone-Boissard et al., 2009). Analytical precision of the halogen analyses is calculated by repeated independent sample preparation and amounts to 2–6% RSD for F analysis and between 10–25% RSD for Cl analysis. The accuracy is controlled by comparing the results on the international reference standards AGV-1 and NIST610 with the recommended values, and is found between 3–12% RSD for F analyses and below 22% RSD for Cl analyses.

Mica varieties for geochemical analyses have been sampled along the different zones of the Manono-Kitotolo pegmatite systems (Tables 1 & 2). Two samples (RG 3113 and RG 16811) have been collected from the exocontact, border zone between a schistose metapelitic host-rock and the pegmatite. Sample RG 3113 is, moreover, affected by late-stage muscovitization (greisen). Samples RG 16727 and RG 16729 are collected from the wall zone; the former sample showing signs of muscovitization. The unaltered K-feldspar subzone of the intermediate zone is represented by samples RG 5826 and RG 9699; while samples RG 8337a and RG 8337b are intensely albitized aliquots of the K-feldspar subzone. Sample RG 15992 is collected from the spodumene subzone of the intermediate zone and sample RG 16005 from the albite-spodume subzone, and as such characterized by albitization. Sample RG 16775 is a lepidolite mica from the most evolved, quartz-rich zone of the pegmatite. Sample RG 16958 is an immature and barren greisen showing relict K-feldspars which are partly affected by muscovitization. Samples RG 16747 and RG 16777 are mature greisens, entirely composed of quartz, muscovite and mineralized in cassiterite.

Micas in the Manono-Kitotolo pegmatite system present relatively small variation in texture and composition. Mica sizes changes from medium in the primary pegmatite units (border, wall, intermediate and quartz core zone) to coarse in the secondary greisen units. All structural formulae for the mica have been calculated with a trioctahedral structure on the basis of 22 oxygens to enable comparison between the mica varieties (cf. Roda-Robles et al., 2012; Table 1) The compositions are classified based on the *feal* (octahedral $Fe_T + Mn + Ti - Al^{VI}$) vs. *mgli* (octahedral Mg–Li) discrimination plot for trioctahedral micas of Tischendorf et al. (2001). The micas belong compositionally to muscovite–lepidolite series of the Al-mica class. With the exception of the lepidolite mica variety, occurring in the quartz core zone, all analyzed micas belong to the muscovite variety. These muscovites present a continuous compositional trend for some major and trace elements from the border to the intermediate zones, with a decrease in the Al and Mg contents and a gradual increase in the F content. In the primary and greisen zones of the Manono-Kitotolo pegmatite system, a continuous evolution from muscovitic to lepidolitic compositions can be observed.

5.2. Trace elements distributions in mica

Alkali metal concentrations and ratios are proven evolutionary proxies for the degree of differentiation of individual pegmatites and of regional pegmatite groups (e.g., Černý and Burt, 1984; Jolliff et al., 1987, 1992; Hulsbosch et al., 2013, 2014). In order to evaluate the alkali metal distribution, the different zones of the Manono-Kitotolo pegmatite system have been classified as primary (or unaltered) if they have not been affected by late-stage albitization or muscovitization metasomatic events (i.e., secondary or altered assemblages). K/Rb vs. Rb and Rb vs. Cs in muscovite from Manono-Kitotolo (Fig. 8) show a progressive evolution from unaltered, primary assemblages starting from the border zone (exocontact), wall zone, intermediate K-feldspar subzone, intermediate spodumene subzone towards lepidolite from the quartz-rich zone. A comparable evolution trend is evidenced from the K/Cs vs. Cs ratios (Fig. 8B), except for sample RG 5826 from the intermediate K-feldspar subzone, which shows an atypical low Cs content for Central African pegmatites (cf. Hulsbosch et al., 2014). Alkali metal contents of altered muscovite associated with albitized zones and of secondary muscovite from greisens vary significantly compared to the concentrations in their unaltered counterparts. For the K-feldspar subzone, Rb concentrations in muscovite from albitized assemblages are relatively constant or have a slight tendency to increase compared to the muscovites of the unaltered K-feldspar subzone (Fig. 8A & C); while Cs concentrations of muscovite associated with albitization are overall lower than primary muscovite of unaltered subzones (i.e., RG 9699; Fig. 8B & C).

6. ^{40}Ar–^{39}Ar dating

Muscovite crystals from three samples have been selected for ^{40}Ar–^{39}Ar age dating, two from the unaltered intermediate zone of the pegmatites and one from a cassiterite-mineralized greisen. A first muscovite sample was taken from the K-feldspar intermediate zone and consists of microcline, albite, muscovite and quartz (RG 9699). The second sample is from the spodumene-intermediate zone and contains spodumene, muscovite, albite and quartz (RG 15993). The ages obtained on these samples should allow to determine the age of the crystallization of the pegmatites, and the associated columbite-tantalite (and primary cassiterite generation) mineralization, prior to the metasomatic alteration. These muscovites are millimeter to centimeter large. Muscovite has also been sampled from a mineralized “greisen” (RG 3554), which allows determination of the age of the metasomatic alteration and the associated secondary cassiterite mineralization. The muscovite flakes of the “greisens” are in general centimeter-scale crystals.

Some of the muscovite crystals have a brown coating composed of Fe-oxides at the edges of the crystals. The muscovite has been crushed gently and only pure muscovite sheets larger than 1 mm have been hand-picked for further analysis. The separates were weighed, wrapped in Al foil and vacuum-encapsulated in quartz vials with the neutron flux monitor Hb3gr ($t = 1073.6 \pm 5.3$ Ma; Jourdan et al., 2006). Nuclear irradiation was carried out on position B2W of the SAFARI-1 reactor at Pelindaba, South Africa, using a time integrated fast neutron flux of $\sim 2 \times 10^{18}$ n cm^2. The J value determined from Hb3gr was 0.01034 ±

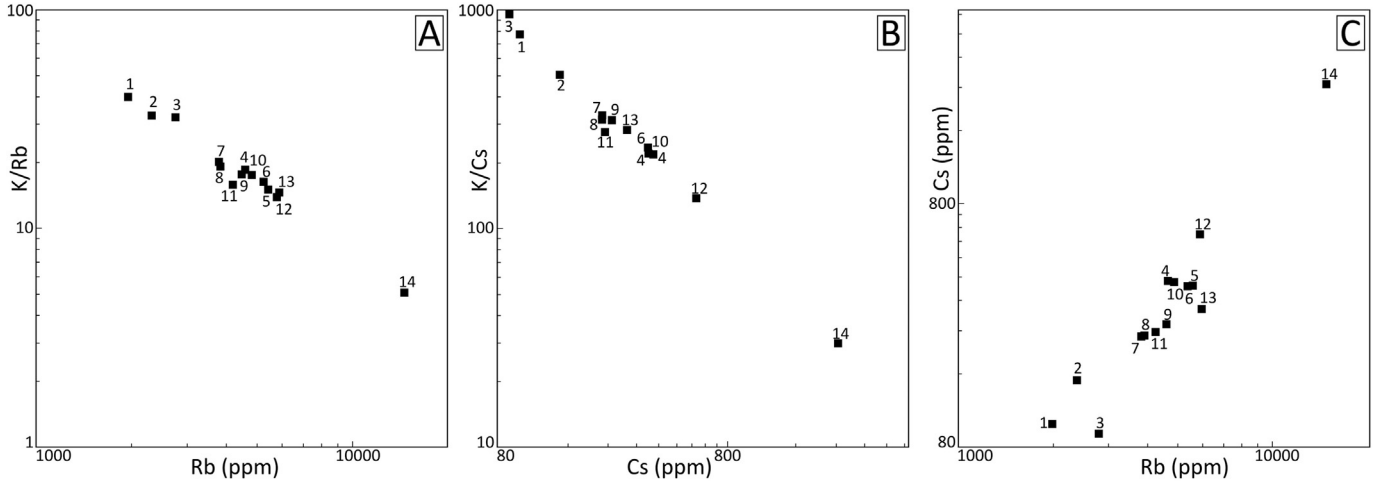

Fig. 8. Alkali metal trends in muscovite from the different internal zones of the Manono-Kitotolo pegmatites: A) K/Rb versus Rb, B) K/Cs versus. Cs and C) Rb versus Cs. Detailed description of the different muscovite samples in association with the identified internal pegmatite zones and alteration assemblages is given in the text.

0.00010 (2σ). The muscovite samples were analyzed by the Ar–Ar step-heating technique using an MS1 mass spectrometer at the University of Manchester, equipped with a Baur–Signer ion source and a Faraday collector. The irradiated samples were heated in a Ta-resistance furnace over the temperature interval of 500 to 1600 °C, using 30 min heating steps. During heating, Ar was purified using a Zr–Al getter at 450 °C. Raw isotope data were corrected for mass discrimination (calibrated using atmospheric argon), radioactive decay and neutron interference. Further experimental details are given by Burgess et al. (2004). Ar–Ar ages were determined from age spectra, using the ISOPLOT/Ex 3.23 software (Ludwig, 2003), and all data are reported at the 2 σ level of uncertainty. The age spectra are plotted in Fig. 9.

Muscovite crystals from the microcline–albite–muscovite–quartz pegmatite (RG 9699) show a plateau age of 938.8 ± 5.1 Ma (54.3% of the released ^{39}Ar) (Fig. 9A), while the muscovite from the spodumene–muscovite–albite–quartz pegmatite (RG 15993) (Fig. 9B) results in a plateau age of 934.0 ± 5.9 Ma (53.7% of the released ^{39}Ar). These ages overlap within error. The muscovite from the greisenized mineralized sample gives a plateau age of 923.3 ± 8.3 Ma (51.6% of the released ^{39}Ar) (Fig. 9C), which is within error similar to the spodumene–muscovite–albite–quartz pegmatite sample, but younger than the microcline–albite–muscovite–quartz pegmatite sample.

7. Stable isotopes

The stable isotopic composition of a quartz sample of a spodumene–muscovite–albite–quartz pegmatite (RG 15993) and quartz and cassiterite from a mineralized greisen sample (RG 3554) has been determined at the Scottish Universities Research Centre (SUERC) in East Kilbride, Scotland. Hand-picking of cleaned grains ensured that no mineral impurities were present. All separates were analyzed for $\delta^{18}O$ using a laser fluorination procedure, involving total sample reaction with excess ClF_3 using a CO_2 laser as a heat source. Reproducibility is around 0.3‰ (1σ). Results were reported as per mil (‰) deviations from the Vienna Standard Mean Ocean Water (V-SMOW) standard. Samples of quartz and cassiterite were selected for measurement of inclusion fluid δD. Although handpicking ensured that mineral separates were pure, it was unavoidable that different fluid generations were sampled. The technique involves decrepitation of fluid inclusion under vacuum using bulk samples (>600 mg quartz) following the technique of Fallick et al. (1987). Data are reported in δD notation as per mil (‰) variations from Vienna Standard Mean Ocean Water (V-SMOW). Reproducibility of this procedure is around 5‰.

The $\delta^{18}O$ value for the quartz sample of a spodumene–muscovite–albite–quartz pegmatite is +10.5‰ V-SMOW, while the δD value is −73.8 V-SMOW. The $\delta^{18}O$ and δD values of the quartz sample of the mineralized greisen are +8.2‰ V-SMOW and −64.7‰, respectively. The $\delta^{18}O$ and δD values of the cassiterite sample of this greisen are +3.5‰ V-SMOW and −78.7‰ V-SMOW, respectively. If isotopic equilibrium is considered between the quartz and cassiterite of the greisen sample, a temperature of 500 °C–550 °C can be calculated (cf. Alderton, 1990; Zheng, 1991; Zhang et al., 1994). Temperatures of 500 °C and more have been proposed for magmatic fluids involved in pegmatite systems (e.g., Ruggieri and Lattanzi, 1992; Sirbescu et al., 2008; Thomas and Spooner, 1988; Thomas et al., 2003). Melt inclusions have been observed in quartz from greisenized samples by Cryns (2013), which could be an indication for this high temperature of formation. However, microthermometric study of a mineralized greisen by Cryns (2013) indicated the predominance of numerous secondary low temperature (T_{hTot} of 120–265 °C) H_2O–NaCl–($MgCl_2$–$CaCl_2$) fluid inclusions which are certainly not magmatic in origin. In addition, the main cassiterite stage present in the greisens is, based on petrographic observations, clearly not a primary magmatic liquidus phase, but crystallized later during metasomatic alteration. These metasomatic fluids are generally interpreted as lower temperature fluids (between 250 and 450 °C; e.g., Kontak and Kyser, 2009; Stemprok, 1987).

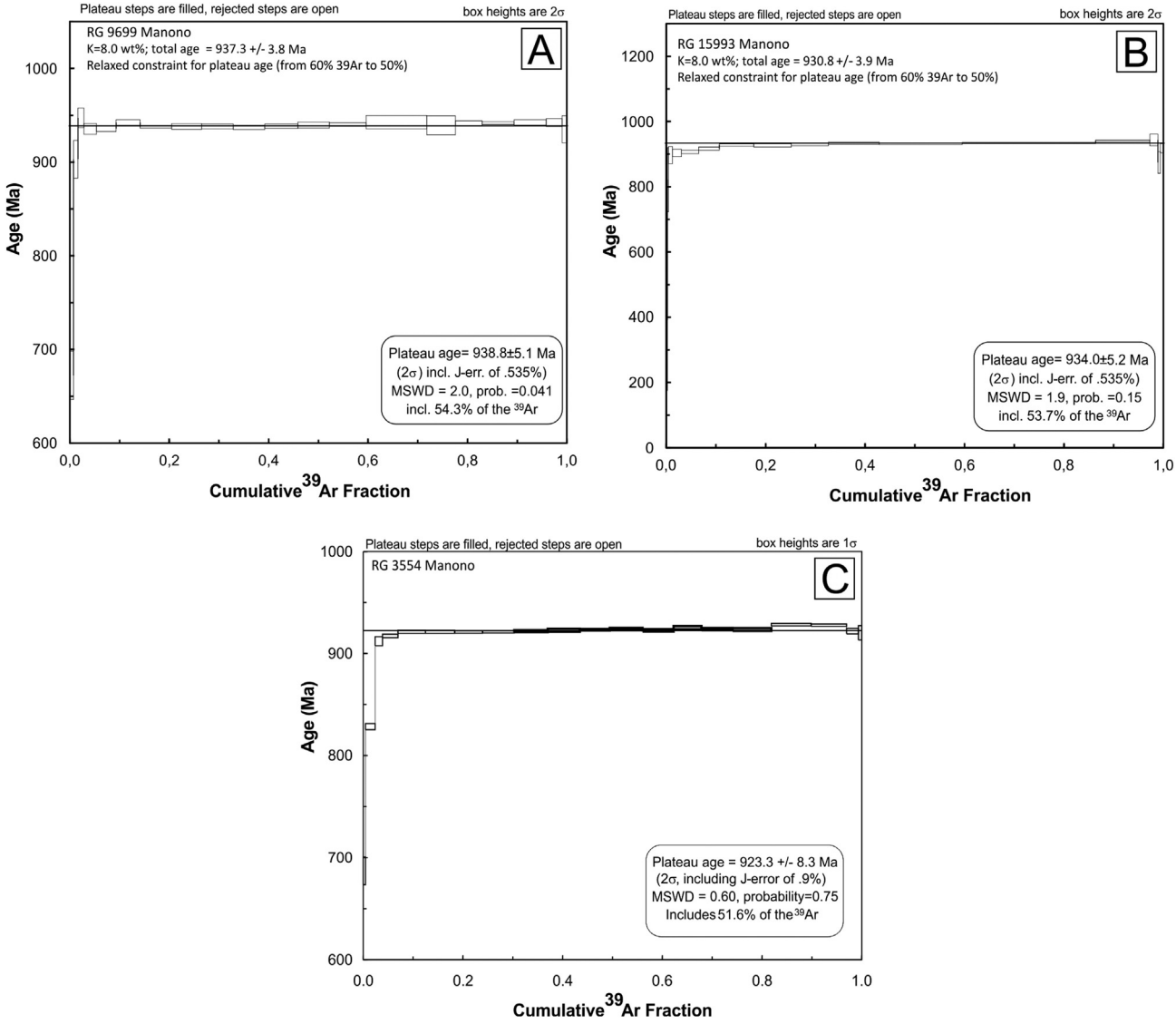

Fig. 9. ^{40}Ar–^{39}Ar spectra of muscovite samples. A. Albite–microcline–muscovite–quartz pegmatite (RG 9699), B. Spodumene–muscovite–albite–quartz pegmatite (RG 15993). C. Greisenized mineralized sample (RG 3554).

By using 550 °C and 350 °C as estimates of the temperature of formation, the ambient isotopic composition of the fluid from which the quartz and cassiterite formed can be calculated (Table 3; Zhang et al., 1994; Zheng, 1991). In a $\delta^{18}O$–δD isotope diagram (cf. Hoefs, 2009), the values of the quartz of the spodumene–muscovite–albite–quartz pegmatite and the quartz and cassiterite of the mineralized greisen for a temperature of 550 °C plot in the field typical for primary magmatic water (Fig. 10). The value of the quartz from the mineralized greisen also falls in the area where there is an overlap of the magmatic and metamorphic field (Fig. 10). For a temperature of 350 °C, the values of the quartz of the spodumene–muscovite–albite–quartz pegmatite and the cassiterite of the mineralized greisen still fall in the magmatic field, while the value of the quartz from the mineralized greisen falls between the field of the primary magmatic/metamorphic field and the meteoric water line (Fig. 10). This corresponds to the microthermometric data of Cryns (2013) that indicated the massive presence of low-temperature secondary fluid inclusions. This all indicates that there is no isotopic equilibrium or cogenetic origin between the quartz and cassiterite from the mineralized greisen and that the temperature of 550 °C cannot be used as an estimate of the formation temperature.

8. Discussion

The Manono-Kitotolo deposit consists of different pegmatite veins that were emplaced along the foliation in metasedimentary rocks and dolerites (Ngulube, 1994). Two structural orientations have been identified in the Manono-Kitotolo area by Ngulube (1994) that have been linked to two regional deformation events (Kokonyangi et al., 2001, 2004). A dominant S1 foliation, parallel to the bedding S0, formed during deformation in a continental arc setting (D1), and has been intersected by a second S2 foliation formed during the D2 deformation of the Kibaran orogeny. This latter deformation compressive event is interpreted as the climax of the Kibaran orogeny at ~1 Ga (Kokonyangi et al., 2001, 2004, 2006), characterized by regional development of NW–SE trending isoclinal meso- and macroscale folds and reverse folds, resulting in crustal thickening. The D2 deformation was, however, not penetrative enough to obliterate the D1 structures, resulting in D1 structures that determine the structural orientation in the Manono-Kitotolo area (Ngulube, 1994). The pegmatites are posterior to the S2 foliation. Based on this spatial relationship, it can be concluded that the Manono-Kitotolo pegmatites were emplaced very late during this deformation event, possibly during the transition from

Table 3
The stable isotopic composition of a quartz sample of spodumene–muscovite–albite–quartz pegmatite (RG 15993), and quartz and cassiterite from a mineralized greisen sample (RG 3554). The ambient isotopic composition of the fluid from which the quartz and cassiterite formed has been calculated for 550 °C and 350 °C (Zhang et al., 1994; Zheng, 1991).

Sample number	Mineral	Paragenesis	$\delta^{18}O_{SMOW}$			δD_{SMOW}
			Measured	550 °C	350 °C	
RG 3554	Quartz	Greisen	8.2	5.7	2.6	−64.7
RG 3554	Cassiterite	Greisen	3.5	7.7	7.4	−78.6
RG 15993	Quartz	Pegmatite	10.5	8	4.9	−73.8

orogenic collapse to extensional tectonics. No exact ages are available for this deformation phase in the Kibara belt. The U–Pb SHRIMP dating of metamorphic zircon overgrowths in the Kisele monzogranite gneiss give an age of 1079 ± 14 Ma, which could be considered as a maximum age of the compressive deformation (Kokonyangi et al., 2004). This is largely consistent with a 1050 ± 50 Ma U–Pb yttrocrasite age in the Mandwe Granite gneiss (Ebenhardt et al., 1956) and a ~1030 Ma U–Pb zircon age in the Fwifwi leuco-monzogranite (Cahen and Snelling, 1966). A minimum age for the D2 deformation event could be deduced from the Rb–Sr age of the E-granites (977 ± 18 Ma in the Mwanza Massif and 966 ± 21 Ma in the Mount Bia Massif; Cahen and Ledent, 1979), since these are unaffected by D2 structures and are attributed to post-collisional relaxation in the KIB (Cahen et al., 1984; Kokonyangi et al., 2001, 2004, 2006).

The Manono-Kitotolo pegmatites have been related to the Lukushi and M'Pete leucogranites that are reddish equigranular, hypidiomorphic and contain abundant tourmaline (Ngulube, 1994). No foliation has been described in this granite generation, compared to the gray colored foliated and porphyric granites and migmatitic granites in the same area. These leucogranites also crosscut the foliated and porphyric granites and occur in the immediate vicinity of the Manono-Kitotolo quarry. In addition, no crosscutting quartz veins and pegmatites are identified in these leucogranites and mineralized pegmatite-like rocks have been identified as cupolas in the upper part of these leucogranites (Ngulube, 1994). Therefore, this third group of leucocratic granites is interpreted to have intruded post-deformation and could be considered to be E granites (cf. Cahen et al., 1984). This younger E-granite generation has in general been considered to be the parental granite of the pegmatite and quartz vein mineralization (cf. Cahen and Ledent, 1979; Kokonyangi et al., 2001, 2004, 2006), mainly based on their

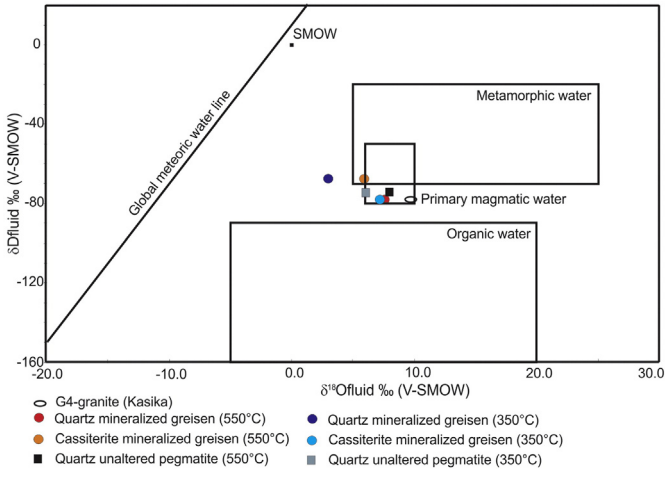

Fig. 10. $\delta^{18}O$–δD plot of the calculated fluid composition of the pegmatite samples from Manono-Kitotolo. Data of Kasika from Dewaele et al. (2007). The global meteoric water line, the composition of seawater and the range of isotopic compositions for metamorphic, magmatic and organic waters are indicated (cf. Sheppard, 1986; Hoefs, 2009). Kasika is situated in the eastern part of the DRC and has been dated by Tack et al. (2010) at 986 ± 10 Ma, and is, therefore, a confirmed G4-granite.

similar age and spatial relation with mineralized pegmatites and quartz veins. However, these Lukushi and M'Pete leucogranites should not necessary be considered as the direct parental granites, since pegmatite melts can originate from deeper granitic sources (Dill, 2015).

Petrographic analysis suggests that the columbite–tantalite mineralization formed during crystallization of the pegmatites. Columbite–tantalite minerals primarily form during the emplacement of pegmatites and not through post-pegmatitic hydrothermal processes because of their low hydrothermal solubility (Linnen, 1998; London, 2008; Van Lichtervelde et al., 2007). It is, therefore, expected that the ages of columbite-tantalite should be similar to the ages of the muscovite associated with the unaltered microcline–albite–muscovite–quartz pegmatite (938.8 ± 5.1 Ma) and the spodumene–muscovite–albite–quartz pegmatite (934.0 ± 5.9 Ma). This is confirmed by U–Pb dating of columbite–tantalite grains that has been performed on crystal fragments from two concentrates from Manono-Kitotolo by conventional TIMS (Melcher et al., 2015), and which gave upper intercept ages of 940.2 ± 5.1 Ma and 947.0 ± 2.8 Ma. A younger U–Pb age on columbite–tantalite overlaps with the Ar–Ar ages obtained on the muscovites of the unaltered pegmatites. The 945–930 Ma time range is therefore considered as the larger period during which the pegmatites and the associated Nb–Ta–Sn and Li mineralization formed.

Crystallization of a single pegmatite body in a granite–pegmatite system spans only a short time interval (London, 2014; Sirbescu et al., 2008; Webber et al., 1999). If the columbite–tantalite U–Pb dates reflect the primary crystallization age of the minerals and by inference emplacement of the pegmatites, then the dates for E-granites should be similar. However, the U–Pb and Ar–Ar ages (945–930 Ma) obtained for the unaltered pegmatites and Nb–Ta–Sn–Li mineralization reported in Melcher et al. (2015) and this study, respectively, are about 40 Ma younger than the Rb–Sr ages mentioned for the so-called parental E-type granites (977 ± 18 Ma in the Mwanza granite, 966 ± 21 Ma in the Monts Bia granite) and the pegmatites (973 ± 13 Ma) by Cahen and Ledent (1979). This time span exceeds most cooling periods of granite–pegmatite systems (London, 2014; Sirbescu et al., 2008; Webber et al., 1999). It should, however, be mentioned that the Rb–Sr ages have been obtained from a mixture of whole-rock and mineral separates and often rehomogenized older tectonized granites have been analyzed (Cahen and Ledent, 1979). In addition, the postulated pegmatite age of Cahen and Ledent (1979) of 973 ± 13 Ma has been calculated based on six different microcline, muscovite and lepidolite samples from different locations in Katanga (Manono, Sofwe and Shienzi), which questions the valor of this age. This implies that the older Rb–Sr ages reported in literature should be treated with care and does not necessarily represent the real age of the parental E-type granites. The recent U–Pb TIMS (Melcher et al., 2015) and Ar–Ar data (this study) could indicate that an age of ~945 Ma may be considered for the E-type granites associated with the Nb–Ta–Sn mineralized pegmatites in Manono-Kitotolo area in Katanga (DRCongo).

The Rb–Sr E-type granite and the pegmatite ages reported by Cahen and Ledent (1979), however, correspond with the U–Pb SHRIMP G4-type granite age in the Karagwe-Ankole belt, reported by Tack et al. (2010). The G4 granites in the Karagwe-Ankole belt are considered as the analogues of the E-type granites in the Kibara belt (Tack et al., 2010). They are the parental granites for the mineralized pegmatites and quartz veins in the Karagwe-Ankole belt (Cahen and Ledent, 1979; Dewaele et al., 2011; Tack et al., 2010). In this belt, recent U–Pb dating (Brinckmann and Lehmann, 1983; Dewaele et al., 2011; Melcher et al., 2015; Romer and Lehmann, 1995) reported pegmatite and Nb–Ta mineralization ages that overlap with the reported ages for the G4-granite. However, younger U–Pb and Ar–Ar ages were also obtained and were interpreted to be possibly caused by a metasomatic/hydrothermal overprint due to more recent tectono-metamorphic events that modified the isotopic system of the columbite–tantalite and the muscovites (Dewaele et al., 2011; Gérards and Ledent, 1976; Ikingura et al., 1992). In the Karagwe-Ankole belt, the Ar–Ar spectra are, however,

largely disturbed and did not show plateau ages, which is not the case for Manono-Kitotolo. In addition, no major tectonic event is known that affected the Manono-Kitololo area after ~1000 Ma (Cahen et al., 1984), different to the case for the Karagwe-Ankole belt where an Ar–Ar plateau age of 593 ± 0.3 Ma was obtained, reflecting the influence of Pan-African tectono-thermal processes in the Western Rift area (Dewaele et al., 2011). Based on these two latter arguments, a younger metamorphic hydrothermal recrystallization history for the newly obtained Ar–Ar ages on muscovites in this study and the U–Pb ages of columbite–tantalite of Melcher et al. (2015) minerals is not retained for the Kibara belt.

Petrographically, the main part of the cassiterite mineralization formed during metasomatic alteration, the so-called greisenization. This greisenization is confined to the pegmatite bodies, which allows us to interpret the pegmatites and the metasomatic alteration as a closed system (Pirajno, 2010). The intensity of greisenization is not everywhere as pervasive, resulting in greisen pockets. Based on petrographic observations it is clear that the greisenization and the associated cassiterite mineralization did not form from a primary magmatic liquidus phase, but from a later metasomatic fluid, altering the primary mineral assemblage. Greisen systems are defined to result from complex late- to post-magmatic metasomatic processes by volatile-rich solutions that affect and take place within a nearly consolidated granite/pegmatite mass (Pirajno, 2010). These volatile-rich fluids are generated during the crystallization of the granitic/pegmatitic fluid by the concentration of H_2O, other volatiles and incompatible elements that remain excluded from the consolidating mass. Fluid inclusion studies of greisen deposits generally confirm the magmatic origin of the hydrothermal fluids, although there are cases which have been interpreted by mixing of magmatic and meteoric water (Pirajno, 2010). Depending on the type of greisen, the nature of the greisenizing fluids can vary from high (600–400 °C and >40 wt.% NaCl eq) to low (~200 °C, 10–15 wt.% NaCl eq) (Roedder, 1984). Although the stable isotope composition of the samples analyzed during this study should be handled with care due to the presence of numerous secondary non-magmatic low temperature fluid inclusions in the quartz from the greisen (Cryns, 2013), the composition of the cassiterite of the mineralized greisen could still reflect a magmatic origin and indicate a close relation between pegmatite/magmatic crystallization and greisenization. As mentioned above, complete crystallization of a single pegmatite body in a granite–pegmatite system occurs over a short time interval (London, 2014; Sirbescu et al., 2008; Webber et al., 1999), implying a similarity in age between pegmatite crystallization and greisenization. The muscovite sample from the mineralized greisen shows a well-defined plateau age at 923.3 ± 8.3 Ma. This age is younger than the Ar–Ar age for the unaltered microcline–albite–muscovite–quartz pegmatite, but partly overlaps within error with the age of the spodumene–muscovite–albite–quartz pegmatite.

Muscovites in albitized units were initially formed during pegmatite crystallization and subsequently affected by the late-stage albitization fluids (cf. Kontak and Kyser, 2009; Dewaele et al., 2007, 2011). In contrast, muscovite of greisenization units were newly formed, precipitating directly from fluids related to greisenization (cf. Stemprok., 1987; Dewaele et al., 2011). As such, both fluid-driven, metasomatic events have the potential to redistribute the initial magmatic Rb and Cs signature of micas. Micas affected by albitization metasomatism show a Cs-depletion compared to their counterparts from unaltered units of the some pegmatite zone. This is consistent with the higher fluid/mineral compatibility of Cs compared to Rb (London, 2005). Fluid-driven albitization causes namely a preferential enrichment of Cs in the metasomatic (albitization) fluid which consequently results in a relative increase of the Rb/Cs ratio in micas from albitization units. Greisen muscovite samples are characterized by overall high-end Rb and Cs concentrations (Fig. 8). In contrast to the altered muscovites from albitization zones, the greisen muscovites are clearly secondary in paragenesis, crystallizing directly from the metasomatic (greisenization) fluid. These late-stage greisenization fluids are extremely enriched in Rb and Cs by excessive fluid-fractionation (cf. Stemprok, 1987; Hulsbosch et al., 2014), and consequently also their precipitation products. Lepidolite (sample RG 16775) is extremely enriched in Rb and Cs (Fig. 8). Their genesis in zoned granitic pegmatites is still debatable: 1) primary, non-replacing lepidolite has been reported (e.g., Brown and Wise, 2001; Antunes et al., 2007) and interpreted as crystallization products from a residual melt; 2) secondary lepidolite can also be observed and formed by the action of late F-bearing aqueous fluids (London, 2008). In zoned pegmatites most of the secondary lepidolite appears as irregular masses, probably as a result of a greisenization process (Roda-Robles et al., 2012). Nonetheless, lepidolite assemblages, either primary or secondary, are typically found close to pegmatite cores which are the latest units to consolidate.

Evaluation of the Zn, Sn, Nb, Ta, and W content in muscovite (Fig. 11) can act as a preliminary exploration vector for these metals in the different internal pegmatite zones of the Manono-Kitotolo deposits (i.e., the border zone or exocontact, wall zone, intermediate K-feldspar subzone, intermediate spodumene subzone and lepidolite from the quartz-rich zone). Zn and Sn (Fig. 11A &B) rise progressively from the primary to the albitized zones, culminating in the greisenized zones. Lepidolite units are low in Zn and Sn. Nb is significantly enriched in the unaltered K-feldspar subzones of the intermediate zone (Fig. 11C), while Ta and W show no preferred enrichment in one of the zones analyzed (Fig. 11D & E).

9. Conclusion

The Manono-Kitotolo pegmatites have been emplaced late during the Kibaran orogeny, probably during the transition from orogenic collapse to extensional tectonics. Different pegmatite veins were injected along the foliation resulting in deposits that extends over a zone of more than 15 km long and with a width of ~800 m, forming the Kitotolo deposit in the southwest and the Manono-Kahungwe deposit in the northeast. The Manono-Kitotolo pegmatites have been linked to the reddish Lukushi and M'Pete leucogranites that have been interpreted as examples of the E-type granites in the Kibara belt. This granite generation has been considered as the parental granite of the rare metal mineralization due to their largely similar age and spatial relation. However, this does not implies that the Lukushi and M'Pete leucogranites are specifically the parental granites of the Manono-Kitotolo pegmatites as pegmatite melts can originate from deeper granitic sources.

The emplacement of the granitic pegmatites along the foliation in the surrounding metasediments and dolerites resulted in an intense alteration, characterized by muscovitization, tourmalinization and silicification. Although obscured by the lack of colored minerals and the high degree of intense weathering, an internal zonation with a border zone, a wall zone, an intermediate zone and core can be established based on the mineralogical composition, grain size and morphology of the samples investigated. The intermediate zone could be divided in different subzones due to the dominance of a specific mineral (e.g., K-feldspar, spodumene). This zonation has been defined as an evolving differentiation trend, as is indicated by the K/Rb vs. Rb and K/Cs vs. Cs ratios in muscovite, which show a progressive evolution from unaltered, primary assemblages starting from the border zone (exocontact), wall zone, intermediate K-feldspar subzone, intermediate spodumene subzone towards lepidolite from the quartz-rich zone. Intense metasomatic alteration characterized by albitization and subsequent greisenization overprinted the primary magmatic zonal assemblages with the formation of albitized units and greisenized zones. Petrographical and geochemical observations indicate that Nb–Ta minerals and spodumene formed prior to the metasomatic alteration and preferentially in the K-feldspar subzones of the intermediate zone, while the main cassiterite mineralization could have formed prior and during the later metasomatic alteration, culminating in the greisen units.

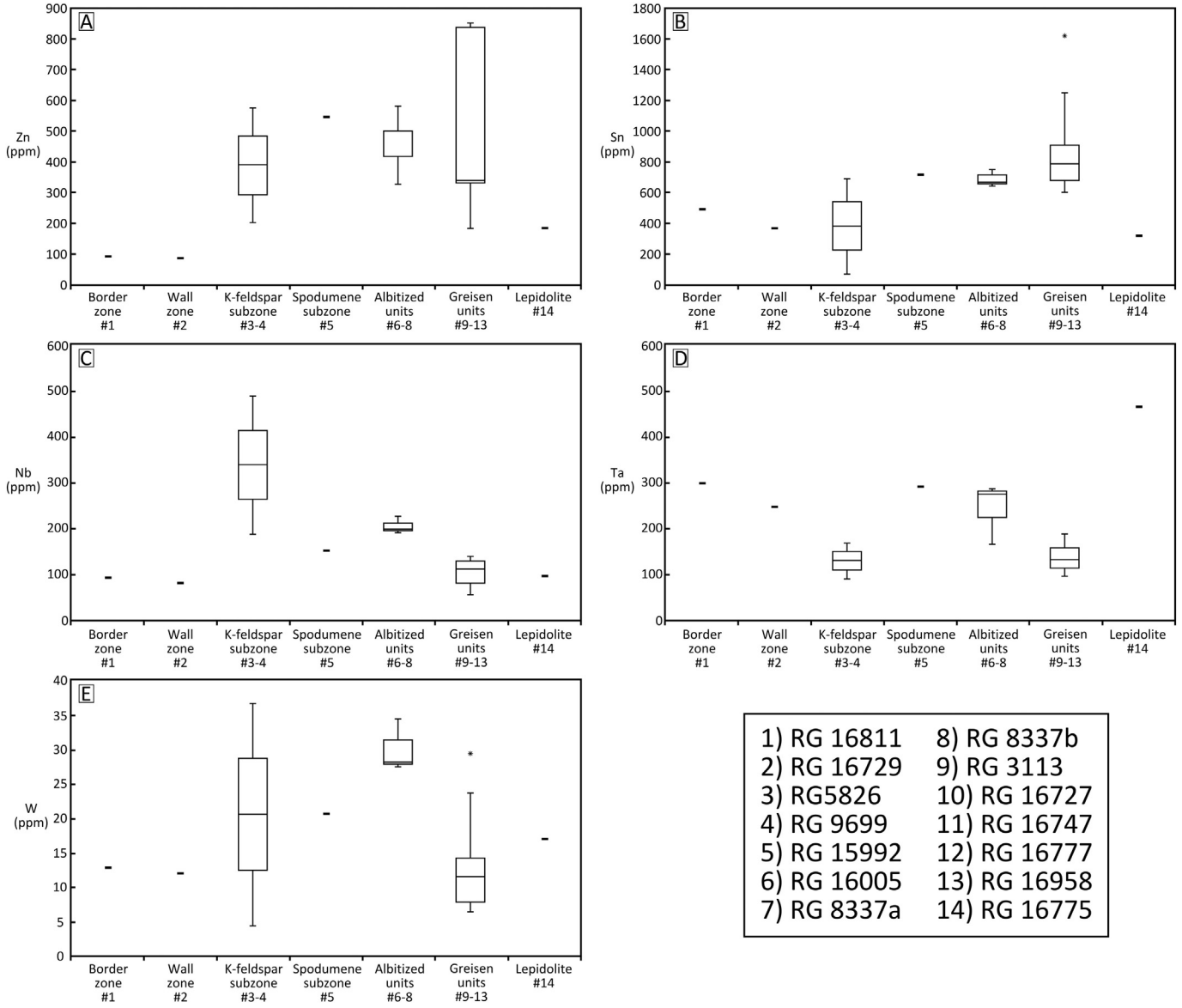

Fig. 11. Metal enrichment trends in muscovite collected from the border zone or exocontact, wall zone, intermediate K-feldspar subzone, intermediate spodumene subzone and lepidolite from the quartz-rich zone; together with albitized and greisenized zones of the Manono-Kitotolo pegmatites: A) Zn, B) Sn, C) Nb, D) Ta and E) W. Detailed description of the different muscovite samples in association with the identified internal pegmatites zones and alteration assemblages is given in the text.

The columbite–tantalite mineralization has been previously dated at 940.2 ± 5.1 Ma and 947 ± 2.8 Ma by U–Pb TIMS. The younger U–Pb age overlaps with the Ar–Ar muscovite ages of the unaltered microcline–albite–muscovite–quartz pegmatite (938.8 ± 5.1 Ma) and the spodumene–muscovite–albite–quartz pegmatite (934.0 ± 5.9 Ma). Since no major post-1000 Ma deformation event is known in the Manono-Kitotolo area and since the Ar–Ar data of the pegmatite samples show proper plateau ages and based on the stable isotope composition, no indication for more recent metasomatic hydrothermal resetting are considered. Therefore, the period between 945 and 930 Ma is interpreted as the time range during which the pegmatites, and the primary magmatic Nb–Ta–(Sn)–Li mineralization, formed at Manono-Kitotolo. Since the crystallization of a pegmatite bodies in a granite–pegmatite system spans only a short time interval, this period should also be the age of the parental granites of the Manono-Kitolo pegmatites. However, granites with such an age have not yet been described in the Kibara belt.

Greisenization has been defined as the result of complex late- to post-magmatic metasomatic processes by volatile-rich solutions that affect and take place within a nearly consolidated granite/pegmatite mass, but a late magmatic origin of the fluids is still preferred. Due to the short period of crystallization of the pegmatite system, a similar but slightly younger age, based on paragenetic arguments, is expected between the pegmatites and the greisens. The stable isotope composition of the cassiterite of the mineralized greisen in this study could still reflect a magmatic origin. However, the mineralized greisen (923.3 ± 8.3 Ma) has an Ar–Ar age which is younger than the age of the unaltered microcline–albite–muscovite–quartz pegmatite (938.8 ± 5.1 Ma), but which partly overlaps within error with the age of the spodumene–muscovite–albite–quartz pegmatite (934.0 ± 5.9 Ma).

Acknowledgments

We gratefully acknowledge Prof. Dr. Bernd Lehmann, Prof. Dr. Encarnación Roda-Robles and Prof. Dr. Harald Dill for their insightful comments that greatly improved this manuscript. Prof. Dr. Harald Dill and Prof. Dr. Franco Pirajno are thanked for the editorial handling of

the manuscript. We are grateful to Dr. Elvira Vassilieva for performing the halogen determinations by ion chromatography. We also thank Herman Nijs for the preparation of the thin and polished sections. Research of Niels Hulsbosch is funded by a Ph.D. grant of the Agency for Innovation by Science and Technology (IWT).

References

Aderca, B., 1950. In: Contribution à la connaissance géologique des gisements stannifèrs Kibariens et à leur métallogénie. Comité Spécial du Katana. 50ième anniversaire, Comptes Rendus du Congrès Scientifique Elisabethville vol.II, tome II, 377–408.

Alderton, D.H.M., 1990. Oxygen fractionation between cassiterite and water. Mineral. Mag. 53, 373–376.

Antunes, I.M.H.R., Neiva, A.M.R., Silva, M.M.V.G., 2007. Geochemistry of minerals from Li-bearing granitic aplite–pegmatite veins of Segura area (Castelo Branco, Portugal). Granitic Pegmatites: The State of the Art — International Symposium, 28–29.

Balcone-Boissard, H., Michel, A., Villemant, B., 2009. Simultaneous determination of fluorine, chlorine, bromine and iodine in six geochemical reference materials using pyrohydrolysis, ion chromatography and inductively coupled plasma-mass spectrometry. Geostand. Geoanal. Res. 33, 477–485.

Bassot, J.P., Morio, M., 1989. Morphologie et mise en place de la pegmatite Kibarienne à Sn, Nb, Ta, Li de Manono (Zaire). Chron. Rech. Min. 496, 41–56.

Brinckmann, J., Lehmann, B., 1983. Exploration de la bastnaésite-monacite dans la région de Gakara, Burundi. Rapport sur la phase 1. Unpublished report, Bujumbura/Hannover, 157 pp.

Brinckmann, J., Lehmann, B., Hein, U., Höhndorf, A., Mussallam, K., Weiser, Th., Timm, F., 2001. La géologie et la minéralisation primaire de l'or de la chaîne Kibarienne, Nord-Ouest du Burundi, Afrique orientale. Geologisches Jahrbuch Reihe D 101 (195 pp.).

Brown, C.D., Wise, M.A., 2001. Internal zonation and chemical evolution of the Black Mountain granite pegmatite. Maine: Can. Mineral. 39 (1), 45–55.

Burgess, R., Kiviets, G.B., Harris, J.W., 2004. $^{40}Ar/^{39}Ar$ age determinations of eclogitic clinopyroxene and garnet inclusions in diamonds from the Venetia and Orapa kimberlites. Lithos 77, 113–124.

Buttgenbach, H., 1933. La thoreaulite, nouvelle espéce minérale. Ann. Soc. Geol. Belg. 56, 327–328.

Cahen, L., 1954. Géologie du Congo Belge. Vaillant Carmanne, Liège.

Cahen, L., Ledent, D., 1979. Précisions sur l'age, la pétrogénèse et la position stratigraphique des “granites à étain” de l'est de l'Afrique Centrale. Bull. Soc. Belg. Géol. 88, 33–49.

Cahen, L., Lepersonne, J., 1967. The Precambrian of the Congo, Rwanda and Burundi. In: Rankama, K. (Ed.), The Geological SystemsThe Precambrian vol. 3. Interscience Publishers, pp. 143–290.

Cahen, L., Snelling, N.J., 1966. The Geochronology of Equatorial Africa. North-Holland Publishing Company, Amsterdam.

Cahen, L., Delhal, J., Deutsch, S., 1967. Rubidium–strontium geochronology of some granitic rocks from the Kibaran belt (Central Katanga, Republic of the Congo). Annales — Serie in 8° — Sciences Géologiques, n°59.

Cahen, L., Delhal, J., Deutsch, S., 1971. Nouvelles données sur l'age de la pétrogénèse des granites post-tectoniques de la chaîne kibarienne, République Démocratique du Congo. Ann. Soc. Geol. Belg. 94, 179–183.

Cahen, L., Snelling, N.J., Delhal, J., Vail, J.R., Bonhomme, M., Ledent, D., 1984. The Geochronology and Evolution of Africa. Clarendon Press, Oxford (512 pp.).

Cameron, E.M., Jahns, R.H., McNair, A.H., Page, L.R., 1949. Internal structures of granitic pegmatites. Econ. Geol. Monogr. 2.

Černý, P., 1991. Rare-element granitic pegmatites. Part I: anatomy and internal evolution of pegmatitic deposits. Geosci. Can. 18, 49–67.

Černý, P., Burt, D.M., 1984. Paragenesis, crystallochemical characteristics, and geochemical evolution of the micas in granite pegmatites. Rev. Mineral. 13, 257–297.

Černý, P., Blevin, P.L., Cuney, M., London, D., 2005. Granite-related ore deposits. In: Hedenquist, J.W., Thompson, J.F.H., Goldfarb, R.J., Richards, J.P. (Eds.), Economic Geology One hundredth Anniversary Volume, pp. 337–370.

Cryns, 2013. Petrographical, mineralogical and geochemical study of the Sn, Nb–Ta, Li–mineralised pegmatites of Manono-Kitotolo, Katanga (D.R.Congo). Unpublished MSc thesis KU Leuven.

De Waele, B., Kampunzu, A.B., Mapani, B., Tembo, F., 2006. The Irumide belt of Zambia. J. Afr. Earth Sci. 46, 36–70.

De Waele, B., Johnso, S.P., Pisarevsky, S.A., 2008. Palaeoproterozoic to Neoproterozoic growth and evolution of the eastern Congo Craton: its role in the Rodinia puzzle. Precambrian Res. 160, 127–141.

De Waele, B., Fitzsimons, I.C.W., Wingate, M.T.D., Tembo, F., Mapani, B., 2009. The geochronological framework of the Irumide Belt of Zambia: a prolonged crustal history along the margin of the Bangweulu Craton. Am. J. Sci. 309, 132–187.

Dewaele, S., Tack, L., Fernandez-Alonso, M., Boyce, A.J., Muchez, P., 2007. Cassiterite and columbite mineralization in pegmatites of the northern part of the Kibara orogen (Central Africa): the Gatumba area (Rwanda). 9th Biennial SGA Meeting: Mineral exploration and research: digging deeper. Irish Association for Economic Geology, Dublin (Ireland), pp. 1489–1492.

Dewaele, S., Henjes-Kunst, F., Melcher, F., Sitnikova, M.A., Burgess, R., Gerdes, A., Fernandez-Alonso, M., De Clercq, F., Muchez, P., Lehmann, B., 2011. Late Neoproterozoic overprinting of the cassiterite and columbite–tantalite bearing pegmatites of the Gatumba area, Rwanda (Central Africa). J. Afr. Earth Sci. 61, 10–26.

Dill, H.G., 2015. Pegmatites and aplites: their genetic and applied ore geology. Ore Geol. Rev. 69, 417–561.

Ebenhardt, P., Geiss, J., Von Gunten, H., Houtermans, F.G., Signer, P., 1956. Mésure de l'âge de l'yttrocrasite de Mitwaba (Katanga) par la méthode de plomb. II: Mesures isotopiques. Bull. Soc. Belg. Géol. 65, 251–255.

ERTS, 1981. Projet de demonstration E.R.T.S. (Etude des Ressources Terrestres par Satellite). Application des images Landsat à l'évaluation des ressources terrestres. Cartographie Géologique au Nord Shaba. Bureau du Président. Unpublished data RMCA.

Fallick, A.E., Jocely, J., Hamilton, P.J., 1987. Oxygen and hydrogen stable isotope systematics in Brazilian agates. In: Rodriquez, C. (Ed.), Geochemistry of the Earth Surface and Processes of Mineral Formation. Instituto de Geologica (CSIC), Madrid, pp. 99–117.

Fernandez-Alonso, M., Theunissen, K., 1998. Airborne geophysics and geochemistry providing insights in the intracontinental evolution of the Mesoproterozoic Kibaran belt (Central Africa). Geol. Mag. 135, 203–216.

Fernandez-Alonso, M., Cutten, H., De Waele, B., Tack, L., Tahon, A., Baudet, D., Barritt, S.D., 2012. The Mesoproterozoic Karagwe-Ankole Belt (formerly the NE Kibara Belt): the result of prolonged extensional intracratonic basin development punctuated by two shortlived far-field compressional events. Precambrian Res. 216–219, 63–86.

Gérards, J., Ledent, D., 1976. Les réhomogénéisations isotopiques d'age Lufilien dans les granites du Rwanda. Musée Royal de l'Afrique Central, Département de Géologie et Minéralogie, Rapport annuel 1975, pp. 91–103.

Goldmann, S., Melcher, F., Gäbler, H.E., Dewaele, S., Clercq, F., Muchez, P., 2013. Mineralogy and trace element chemistry of ferberite/reinite from tungsten deposits in Central Rwanda. Minerals 3, 121–144.

Hoefs, J., 2009. Stable Isotope Geochemistry. 6th edition. Springer-Verlag, Berlin-Heidelberg, p. 285.

Hulsbosch, N., Hertogen, J., Dewaele, S., André, L., Muchez, Ph., 2013. Petrographic and mineralogical characterisation of fractionated pegmatites culminating in the Nb–Ta–Sn pegmatites of the Gatumba area (western Rwanda). Geol. Belg. 16, 105–117.

Hulsbosch, N., Hertogen, J., Dewaele, S., André, L., Muchez, P., 2014. Alkali metal and rare earth element evolution of rock-forming minerals from the Gatumba area pegmatites (Rwanda): quantitative assessment of crystal-melt fractionation in the regional zonation of pegmatite groups. Geochim. Cosmochim. Acta 132, 349–374.

Ikingura, J.R., Reynolds, P.H., Watkinson, D.H., Bell, K., 1992. $^{40}Ar/^{39}Ar$ dating of micas from granites of NE Kibaran belt (Karangwe-Ankolean), NW Tanzania. J. Afr. Earth Sci. 15, 501–511.

Johnson, S.P., Rivers, T., De Waele, B., 2005. A review of the Mesoproterozoic to early Palaeozoic magmatic and tectonothermal history of south-central Africa: implications for Rodinia and Gondwana. J. Geol. Soc. 162, 433–450.

Johnson, S.P., De Waele, B., Evans, D., Banda, W., Tembo, F., Milton, J.A., Tani, K., 2007. Geochronology of the Zambezi supracrustal sequence, Southern Zambia: a record of Neoproterozoic divergent processes along the Southern Margin of the Congo Craton. J. Geol. 115, 355–374.

Jolliff, B.L., Papike, J.J., Shearer, C.K., 1987. Fractionation trends in mica and tourmaline as indicators of pegmatite internal evolution: Bob Ingersoll pegmatite, Black Hills, South Dakota. Geochim. Cosmochim. Acta 51, 519–534.

Jolliff, B.L., Papike, J.J., Shearer, C.K., 1992. Petrogenetic relationships between pegmatite and granite based on geochemistry of muscovite in pegmatite wall zones, Black Hills, South Dakota, USA. Geochim. Cosmochim. Acta 56, 1915–1939.

Jourdan, F., Verati, C., Feraud, G., 2006. Intercalibration of the Hb3gr $^{40}Ar/^{39}Ar$ dating standard. Chem. Geol. 231, 77–189.

Kabete, J.M., Groves, D.I., McNaughton, N.J., Mruma, A.H., 2012. A new tectonic and temporal framework for the Tanzanian Shield: implications for gold metallogeny and undiscovered endowment. Ore Geol. Rev. 37.

Kampunzu, A.B., Rumvegeri, B.T., Kapenda, D., Lubala, R.T., Caron, J.P.H., 1986. Les Kibarides d'Afrique centrale et orientale: une chaîne de collision. UNESCO Geol. Dev. Newslett. 5, 125–137.

Klerkx, J., Liégeois, J.P., Lavreau, J., Theunissen, K., 1984. Granitoides kibariens précoces et tectonique tangentielle au Burundi: magmatisme bimodal lié à une distension crustale. In: Klerkx, J., Michot, J. (Eds.), African Geology, A Volume in Honour of L. Cahen. Musée Royale d'Afrique Centrale, Tervuren, pp. 29–46.

Klerkx, J., Liégeois, J.P., Lavreau, J., Claessens, W., 1987. Crustal evolution of the northern Kibaran Belt, Eastern and Central Africa. In: Kröner, A. (Ed.), Proterozoic lithospheric evolution. Geodynamics Series (American Geophysics Union) 17, pp. 217–233.

Kokonyangi, J., Okudaira, T., Kampunzu, A.B., Yoshida, M., 2001. Geological evolution of the Kibarides Belt, Mitwaba, democratic republic of Congo, Central Africa. Gondwana Res. 4, 663–664.

Kokonyangi, J.W., Armstrong, R., Kampunzu, A.B., Yoshida, M., Okudaira, T., 2004. U–Pb zircon geochronology and petrology of granitoids from Mitwaba (Katanga, Congo): implications for the evolution of the Mesoproterozoic Kibaran belt. Precambrian Res. 132, 79–106.

Kokonyangi, J.W., Kampunzu, A.B., Armstrong, R., Yoshida, M., Okudaira, T., Arima, M., Ngulube, D.A., 2006. The Mesoproterozoic Kibaride belt (Katanga, D.R. Congo). J. Afr. Earth Sci. 46, 1–35.

Kontak, D.J., Kyser, T.K., 2009. Nature and origin of an LCT-suite pegmatite with late-stage sodium enrichment, Brazil Lake, Yarmouth County, Nova Scotia. II. Implications of stable isotopes (d18O, dD) for magma source, internal crystallization and nature of sodium metasomatism. Can. Mineral. 47 (4), 745–764.

Kristiansen, R., 2001. Sjeldne tantalniobater fra Sentral-Afrika. eksotiske minerallokaliteter II (Exotic mineral-locations II). STEIN 28 (2), 21–28.

Laghmouch, M., Fernandez, M., Dewaele, S., 2012. Uniform GIS-compilation (1: 750.000) of a geological map of the Kibara fold belt, Katanga, Democratic Republic of Congo (DRC). 4th International Geologica Belgica Meeting — Moving Plates and melting Icecaps, processes and forcing factors in Geology. Book of abstracts. 236.

Landa, L., Karpoff, D., Claeys, E., 1950. Géologie du gisement de Manono. Comité Spécial du Katanga, 50ième anniversaire. Comptes Rendus du Congrès Scientifique Elisabethville vol. II, tome II, pp. 333–343.

Lehmann, B., Halder, S., Ruzindana Munana, J., de la Paix Ngizimana, J., Biryabarema, M., 2014. The geochemical signature of rare-metal pegmatites in Central Africa: magmatic rocks in the Gatumba tin–tantalum mining district, Rwanda. J. Geochem. Explor. 144, 528–538.

Linnen, R.L., 1998. The solubility of Nb–Ta–Zr–Hf–W in granitic melts with Li and Li + F: constraints for mineralization in rare metal granites and pegmatites. Econ. Geol. 93, 1013–1025.
London, D., 2005. Geochemistry of alkali and alkaline earth elements in ore-forming granites, pegmatites, and rhyolites. In: Linnen, R.L., Samson, I.M. (Eds.), Volume GAC Short Course Notes 17: Rare-Earth Geochemistry and Mineral Deposits, Geological Association of Canada, pp. 17–43.
London, D., 2008. PegmatitesThe Canadian Mineralogist, Special Publication 10. Mineralogical Association of Canada (347 pp.).
London, D., 2014. A petrologic assessment of internal zonation in granitic pegmatites. Lithos 184–187, 74–104.
Ludwig, K., 2003. Isoplot/Ex, Version 3: A Geochronological Toolkit for Microsoft Excel. Geochronology Center, Berkeley, USA.
Melcher, F., Graupner, T., Gäbler, H.E., Sitnikova, M., Henjes-Kunst, F., Oberthür, T., Gerdes, A., Dewaele, S., 2015. Tantalum-(niobium–tin) mineralisation in African pegmatites and rare metal granites: constraints from Ta–Nb oxide mineralogy, geochemistry and U–Pb geochronology. Ore Geol. Rev. 64, 667–719.
Ngulube, A.D., 1994. La pegmatite de Manono (Zaire) et sa place dans la métallogénie Kibarienne. Unpublished PhD thesis of Laboratoire de Pétrologie, Université de Nancy I.
Norton, J.J., 1983. Sequence of mineral assemblages in differentiated granitic pegmatites. Econ. Geol. 78, 854–874.
Pirajno, F., 2010. Hydrothermal Processes and Mineral Systems. Springer Science + Business Media B.V.
Pohl, W., 1994. Metallogeny of the northeastern Kibara belt, Central Africa — recent perspectives. Ore Geol. Rev. 9, 105–130.
Pohl, W., Günther, M.A., 1991. The origin of Kibaran (late Mid-Proterozoic) tin, tungsten and gold quartz vein deposits in Central Africa: a fluid inclusion study. Mineral. Deposita 26, 51–59.
Pohl, W.L., Biryabarema, M., Lehmann, B., 2013. Early Neoproterozoic rare metal (Sn, Ta, W) and gold metallogeny of the Central Africa Region: a review. Appl. Earth Sci. 122, 66–82.
Roda-Robles, E., Pesquera, A., Gil-Crespo, P., Torres-Ruiz, J., 2012. From granite to highly evolved pegmatite: A case study of the Pinilla de Fermoselle granite–pegmatite system (Zamora, Spain). Lithos 153, 192–207.
Roedder, E., 1984. Fluid Inclusions, Reviews in Mineralogy 12. Mineralogical Society of America (644 pp.).
Romer, R.L., Lehmann, B., 1995. U–Pb columbite–tantalite age of Neoproterozoic Ta–Nb mineralisation in Burundi. Econ. Geol. 90, 2303–2309.
Rossetti, F., Cozzupoli, D., Phillips, D., 2007. Compressional reworking of the East African Orogen in the Uluguru Mountains of eastern Tanzania at c. 550 Ma: implications for the final assembly of Gondwana. Terra Nova 20 (1), 59–67.
Ruggieri, G., Lattanzi, P., 1992. Fluid inclusion studies on Mt. Capanne pegmatites, Isola d'Elba, Tuscany, Italy. Eur. J. Mineral. 4, 1085–1096.
Rumvegeri, B.T., 1991. Tectonic significance of Kibaran structures in central and eastern Africa. J. Afr. Earth Sci. 13, 267–276.
Sheppard, S.M.F., 1986. Characterization and isotopic variations in natural waters. In: Valley, J.W., Taylor, H.P.J., O'Neil, J.R. (Eds.), Stable Isotopes in High Temperature Geological Processes. Reviews in Mineralogy 16, pp. 165–184.
Sirbescu, M.L.C., Hartwick, E.E., Student, J.J., 2008. Rapid crystallization of the Animikie Red Ace Pegmatite, Florence county, northeastern Wisconsin: inclusion microthermometry and conductive-cooling modeling. Contrib. Mineral. Petrol. 156, 284–305.
Stemprok, M., 1987. Greisenization (a review). Geogr. Rundsch. 76, 169–175.
Tack, L., Wingate, M., De Waele, B., Meert, J., Belousova, E.A., Griffin, B., Tahon, A., Fernandez-Alonso, 2010. The 1375 Ma "Kibaran event" in Central Africa: Prominent emplacement of bimodal magmatism under extensional regime. Precambrian Res. 180, 63–84.
Theunissen, K., 1988. Kibaran thrust fold belt (D1–2) and shear belt (D2'). IGCP No 255 Bulletin/Newsletter 1. TU Braunschweig and RMCA, Tervuren, pp. 55–64.
Theunissen, K., 1989. On the Ruzuzian basement rise in the Kibara belt of Northern lake Tanganyika. Collision Belt Geometry or Restraining Bend Emplaced in the Later Kibaran Strike Slip Environment. IGCP newsletter, n°255 2, pp. 85–92.
Thomas, A.V., Spooner, E.T.C., 1988. Fluid inclusions in the system H_2O–CH_4–NaCl–CO_2 from metasomatic tourmaline within the border unit of the Tanco zoned granitic pegmatite, S.E. Manitoba. Geochim. Cosmochim. Acta 52, 1065–1075.
Thomas, R., Förster, H.J., Heinrich, W., 2003. The behaviour of boron in a peraluminous granite–pegmatite system and associated hydrothermal solutions: a melt and fluid inclusion study. Contrib. Mineral. Petrol. 144, 457–472.
Thoreau, J., 1950. La pegmatite stannifère de Manono (Katanga). Comité Spécial du Katanga, 50ième anniversaire. Comptes Rendus du Congrès Scientifique Elisabethville vol. II, tome II, pp. 344–376.
Tindle, A.G., Webb, P.C., 1990. Estimation of lithium contents in trioctahedral micas using microprobe data — application to micas from granitic rocks. Eur. J. Mineral. 2, 595–610.
Tischendorf, G., Förster, H.-J., Gottesmann, B., Trumbull, R.B., 1997. On Li-bearing micas: estimating Li from electron microprobe analyses and an improved diagram for graphical representation. Mineral. Mag. 61, 809–834.
Tischendorf, G., Gottesmann, B., Förster, H.-J., 2001. Minor- and trace-element composition of trioctahedral micas: a review. Mineral. Mag. 65, 249–276.
Van Lichtervelde, M., Salvi, S., Béziat, D., 2007. Textural features and chemical evolution in tantalum oxides: magmatic versus hydrothermal origins for Ta mineralization in the Tanco Lower Pegmatite, Manitoba, Canada. Econ. Geol. 102, 257–276.
Webber, K.L., Simmons, Wm.B., Falster, A.U., Foord, E.E., 1999. Cooling rates and crystallization dynamics of shallow level pegmatite–aplite dikes, San Diego County, California. Am. Mineral. 708–717.
Zhang, L.G., Liu, J.X., Chen, Z.S., Zhou, H.B., 1994. Experimental investigations of oxygen isotope fractionation in cassiterite and wolframite. Econ. Geol. 89, 150–157.
Zheng, Y.F., 1991. Calculation of oxygen isotope fractionation in metal oxides. Geochim. Cosmochim. Acta 55, 2299–2307.